





Neutron Star in Covariant $f(Q)$ gravity

Muhammad Azzam Alwan ^{a,b}, Tomohiro Inagaki ^{a,c,d}, B. Mishra ^e and S.A. Narawade ^e

^aGraduate School of Advanced Science and Engineering, Hiroshima University, Higashi-Hiroshima 739-8526, Japan

^bResearch Center for Quantum Physics, National Research and Innovation Agency (BRIN), Tangerang Selatan 15314, Indonesia

^cInformation Media Center, Hiroshima University, Higashi-Hiroshima 739-8521, Japan

^dCore of Research for the Energetic Universe, Hiroshima University, Higashi-Hiroshima 739-8526, Japan

^eDepartment of Mathematics, Birla Institute of Technology and Science-Pilani, Hyderabad Campus, Hyderabad-500078, India.

E-mail: azzam-alwan@hiroshima-u.ac.jp, inagaki@hiroshima-u.ac.jp, bivu@hyderabad.bits-pilani.ac.in, shubhamn2616@gmail.com

Abstract. Assuming static and spherically symmetric stars with perfect fluid matter, we used realistic equations of state to study neutron stars in covariant $f(Q)$ gravity. The structure profiles and properties of neutron stars such as mass, radius and compactness are obtained through numerical methods using quadratic, exponential, and logarithmic $f(Q)$ models. The results indicate that nonmetricity affects the interior profile deviations of the star, which in turn influence the properties of stars, as illustrated in the mass-radius relation diagram. This effect allows the star to accommodate either more or less matter compared to GR, resulting in a different total mass. For the quadratic model, we cannot generate larger masses, whereas the other two models can give consistent results for both smaller and larger masses of the observed stars. By tuning model parameters, we obtain $\mathcal{M} - \mathcal{R}$ diagrams that are compatible with observational constraints from NICER and LIGO.

Keywords: $f(Q)$ gravity, neutron stars, Mass-Radius relation

Contents

1	Introduction	1
2	Mathematical Formalism	3
2.1	Covariant Formulation of $f(Q)$ Theory	3
2.2	TOV Equations in Covariant $f(Q)$ gravity	4
3	$f(Q)$ Models	5
3.1	$f(Q) = Q + \alpha Q^2$	5
3.2	$f(Q) = Q + \alpha e^{\beta Q}$	6
3.3	$f(Q) = Q - \alpha \ln(1 - \beta Q)$	7
4	Neutron Star Structure for $f(Q)$ Models	8
4.1	Boundary and Junction Conditions	8
4.2	Numerical Solutions	10
4.3	Mass-Radius Relation	13
5	Discussion	19
6	Conclusions	20
A	Energy-Momentum Conservation	22
B	Recovering TOV GR	23

1 Introduction

The geometrical modification of General Relativity (GR) has become inevitable post supernovae observations and other cosmological observations [1–4]. Extending and modifying GR presents a promising approach for addressing issues at both early and late cosmological epochs. GR traditionally employs Riemannian geometry, specifying the affine connection on the spacetime manifold to be metric compatible, specifically the Levi-Civita connection. However, different choices of affine connections on a manifold can lead to distinct but equivalent descriptions of gravity, potentially offering new insights [5, 6]. The Levi-Civita connection chosen by GR imposes that except curvature R , the other two fundamental geometrical objects, the nonmetricity Q and torsion T , should both vanish. By relaxing these constraints, one can develop theories of gravity based on non-Riemannian geometry where curvature, torsion, and nonmetricity do not all necessarily vanish. For instance, by selecting a connection where both curvature and nonmetricity vanish while allowing torsion to be non-zero, one can formulate the Teleparallel Equivalent of GR (TEGR) [7, 8]. Alternatively,

a flat spacetime manifold with non-vanishing nonmetricity but no torsion leads to the Symmetric Teleparallel formulation of GR (STGR) [9–16], in which a nonmetricity Q mediates gravitational interaction.

The symmetric teleparallel gravity has evolved into coincident gravity or $f(Q)$ gravity [Jimenez et al [14]]. As extended gravity theories have been emphasized in modern cosmology, alternative geometries are also being investigated. There are several works done in this gravity pertaining to cosmological implications in recent years, Ref. [17–30]. In all of these studies, coincident gauges and line elements were used in Cartesian coordinates. Because of this specific choice, the covariant derivative is reduced to a partial derivative, simplifying calculations. However, the equations for pressure and energy are identical to those for $f(T)$. Regardless of whether the Universe is flat [31–33] or curved [34–37], the $f(Q)$ theory with no coincident gauge attracts increased attention. As the Friedmann equations have been modified [34], the new gauge choices could affect the cosmological dynamics. As a result of the $f(Q)$ theory, the flat Universe always evolves in an unstable radiation era followed by a matter era and then a stable de-Sitter phase with a nontrivial affine connection [32]. By providing dark energy candidates, the $f(Q)$ theory can alleviate the cosmological constant problem. An affine connection could result in early-time acceleration following the inflationary period of the Universe [33]. When taking into account non-zero spatial curvature, the early Universe might undergo a curvature-dominated phase. Furthermore, an open Universe might exhibit a peak in curvature density during intermediate times, according to [36].

Besides its applications in cosmology, $f(Q)$ gravity has also been applied to compact astrophysical objects [38–41]. In this paper, we will discuss one of the compact objects, neutron stars (NS). These relativistic stars, which can be described by GR, serve as natural laboratories for studying high-density nuclear matter. Due to their extreme densities, strong gravitational fields, and the abundance of observational data that can be obtained, such as massive pulsar from Neutron star Interior Composition Explorer (NICER) [42–44] and gravitational wave (GW) events from collaboration of Laser Interferometer Gravitational-Wave Observatory (LIGO) and Virgo Gravitational Wave Interferometer (Virgo) [45, 46], neutron stars provide a good testing ground for both GR and modified gravity theories. The equation of state (EoS) for nuclear matter, which describes the relationship between density, pressure, and temperature, is key to understanding their properties and behavior [47–50]. By examining the mass-radius relations, tidal deformations, and rotational dynamics of neutron stars [51–53], we can explore the validity of these theories under conditions that are inaccessible in the laboratory.

In addition to serving as testing grounds, modified gravity theories also help describe observational evidence that cannot be fully explained by GR. Several astrophysical observations have confirmed the existence of binary systems with NS having mass values that violate the Chandrasekhar limit for non-rotating degenerate stars to maintain stability [54], indicating that neutron stars can possess significantly larger masses than previously predicted [55–58]. For example, modified gravity theories such as $f(R)$ gravity [59–63] and $f(T)$ gravity [64–67], can accommodate larger neutron star masses than GR, making them

more flexible in meeting various observational constraints. In contrast to the other two trinity theories of gravity, there are still relatively few studies of neutron stars in $f(Q)$ gravity such as [68]. They have used the polytropic EoS to calculate the structure and mass-radius relation for $f(Q) = Q + \alpha Q^2$ model. This study shows that $f(Q)$ gravity can accommodate massive star until $> 3M_\odot$. In this work, we are motivated to calculate the profile of NS that includes the interior and exterior solutions of the stars. Also, we will obtain the properties of along with the compactness of the stars with $f(Q)$ covariant formulation.

The paper is organized as: Section 2 gives the covariant formalism of $f(Q)$ gravity and the derivation of gravitational field equations along with the TOV equation for $f(Q)$ gravity using the spherically symmetric metric. Section 3 explains the forms of the $f(Q)$ models that we study. The mass-radius relation and the neutron star structure using the numerical solution for the $f(Q)$ models are analysed in the section 4. In section 5, we discuss about the role of the nonmetricity Q in the formation of the neutron stars. Also this section dedicated to the shortcomings occurring to form the neutron star using the considered $f(Q)$ models. The conclusions are presented in section 6.

2 Mathematical Formalism

2.1 Covariant Formulation of $f(Q)$ Theory

The general affine connection can be decomposed into Levi-Civita connection $\left(\left\{\begin{smallmatrix} \lambda \\ \mu\nu \end{smallmatrix}\right\}\right)$, contortion $\left(K^\lambda_{\mu\nu}\right)$ and disformation $\left(L^\lambda_{\mu\nu}\right)$ as,

$$\Gamma^\lambda_{\mu\nu} = \left\{\begin{smallmatrix} \lambda \\ \mu\nu \end{smallmatrix}\right\} + K^\lambda_{\mu\nu} + L^\lambda_{\mu\nu}, \quad (2.1)$$

where

$$\left\{\begin{smallmatrix} \lambda \\ \mu\nu \end{smallmatrix}\right\} = \frac{1}{2}g^{\lambda\alpha} \left(\partial_\mu g_{\alpha\nu} + \partial_\nu g_{\alpha\mu} - \partial_\alpha g_{\mu\nu}\right), \quad K^\lambda_{\mu\nu} = \frac{1}{2} \left(T^\lambda_{\mu\nu} + T_\mu^\lambda{}_\nu + T_\nu^\lambda{}_\mu\right),$$

$$L^\lambda_{\mu\nu} = \frac{1}{2} \left(Q^\lambda_{\mu\nu} - Q_\mu^\lambda{}_\nu - Q_\nu^\lambda{}_\mu\right).$$

The torsion tensor $\mathcal{T}^\lambda_{\mu\nu}$, as well as the nonmetricity tensor $Q_{\lambda\mu\nu}$, are respectively presented for a spacetime equipped with the metric tensor $g_{\mu\nu}$ and the affine connection $\Gamma^\lambda_{\mu\nu}$.

$$\mathcal{T}^\lambda_{\mu\nu} := \Gamma^\lambda_{\mu\nu} - \Gamma^\lambda_{\nu\mu} \quad Q_{\lambda\mu\nu} := \nabla_\lambda g_{\mu\nu} = \partial_\lambda g_{\mu\nu} - \Gamma^\alpha_{\lambda\mu} g_{\alpha\nu} - \Gamma^\alpha_{\lambda\nu} g_{\alpha\mu}. \quad (2.2)$$

The nonmetricity scalar is defined as $Q = Q_{\lambda\mu\nu} P^{\lambda\mu\nu}$. The $P^\lambda_{\mu\nu}$ is called as nonmetricity conjugate and given as

$$P^\lambda_{\mu\nu} = -\frac{1}{4}Q^\lambda_{\mu\nu} + \frac{1}{4} \left(Q_\mu^\lambda{}_\nu + Q_\nu^\lambda{}_\mu\right) + \frac{1}{4}Q^\lambda g_{\mu\nu} - \frac{1}{8} \left(2\tilde{Q}^\lambda g_{\mu\nu} + \delta_\mu^\lambda Q_\nu + \delta_\nu^\lambda Q_\mu\right). \quad (2.3)$$

A different definition of $Q = -Q_{\lambda\mu\nu} P^{\lambda\mu\nu}$ has been proposed in the literature, which changes the sign of the nonmetricity scalar Q . This is important to consider while comparing different $f(Q)$ results. STEGR (symmetric teleparallel equivalent) of GR can be produced if this

nonmetricity scalar Q replaces the Ricci scalar R in the Einstein-Hilbert action. Because symmetric teleparallel theory is equivalent to GR, it inherits the same ‘dark’ problem as general GR, so a modified $f(Q)$ gravity was introduced, in a similar manner to extending GR through a modified $f(R)$ theory. The components of the connection in eq. (2.1) can be rewritten as,

$$\Gamma^\lambda{}_{\mu\beta} = \frac{\partial y^\lambda}{\partial \xi^\rho} \partial_\mu \partial_\beta \xi^\rho. \quad (2.4)$$

In the above equation, $\xi^\lambda = \xi^\lambda(y^\mu)$ is an invertible relation and $\frac{\partial y^\lambda}{\partial \xi^\rho}$ is the inverse of the corresponding Jacobian [20]. This situation is called a coincident gauge, where there is always a possibility of getting a coordinate system with connections $\Gamma^\lambda{}_{\mu\nu}$ equaling zero. Hence, in this choice, the covariant derivative ∇_λ reduces to the partial derivative ∂_λ i.e. $Q_{\lambda\mu\nu} = \partial_\lambda g_{\mu\nu}$. Thus, it is clear that the Levi-Civita connection $\left(\left\{\begin{smallmatrix} \lambda \\ \mu\nu \end{smallmatrix}\right\}\right)$ can be written in terms of the disformation tensor $L^\alpha{}_{\mu\nu}$ as $\left(\left\{\begin{smallmatrix} \lambda \\ \mu\nu \end{smallmatrix}\right\}\right) = -L^\lambda{}_{\mu\nu}$. By varying the action term [14, 69]

$$S = \int \frac{1}{2\kappa} f(Q) \sqrt{-g} d^4x + \int \mathcal{L}_m \sqrt{-g} d^4x, \quad (2.5)$$

with respect to the metric tensor, we can obtain the field equation

$$\frac{2}{\sqrt{-g}} \nabla_\lambda \left(\sqrt{-g} f_Q P^\lambda{}_{\mu\nu} \right) - \frac{1}{2} g_{\mu\nu} f + f_Q (P_{\mu\lambda\alpha} Q_{\nu}{}^{\lambda\alpha} - 2Q_{\lambda\alpha\mu} P^{\lambda\alpha}{}_{\nu}) = \kappa \mathcal{T}_{\mu\nu}. \quad (2.6)$$

Using this field equation, the covariant formulation has been developed and used effectively in studying geodesic deviations and cosmological phenomena [31, 68–70],

$$f_Q \mathring{G}_{\mu\nu} + \frac{1}{2} g_{\mu\nu} (Q f_Q - f) + 2f_Q Q P^\lambda{}_{\mu\nu} \mathring{\nabla}_\lambda Q = \kappa \mathcal{T}_{\mu\nu}, \quad (2.7)$$

where, f_Q is derivative of f with respect to Q and $\mathring{G}_{\mu\nu} = R_{\mu\nu} - \frac{1}{2} g_{\mu\nu} R$, with $R_{\mu\nu}$ and R are the Riemannian Ricci tensor and scalar respectively which are constructed by the Levi-Civita connection. For a linear form of $f(Q)$ function, the above equation reduces to GR. Variation of eq. (2.4) with respect to the connection, we can derive the equation of motion for the nonmetricity scalar as,

$$\nabla_\mu \nabla_\nu \left(\sqrt{-g} f_Q P^{\mu\nu}{}_\lambda \right) = 0. \quad (2.8)$$

2.2 TOV Equations in Covariant $f(Q)$ gravity

Here, we are taking non-coincident gauge i.e. $\Gamma^\lambda{}_{\mu\nu} \neq 0$ into account and considering the spherically symmetric metric form as,

$$ds^2 = -e^{A(r)} dt^2 + e^{B(r)} dr^2 + r^2 (d\theta^2 + \sin^2\theta d\phi^2), \quad (2.9)$$

with perfect fluid matter with $T_{\mu\nu} = \text{diag}\{-\rho c^2, p, p, p\}$ as ideal energy-momentum tensor. Using the Levi-Civita connection eq. (2.1) and the assumption of arbitrary affine connections, we can obtain all non-vanishing components of connections as,

$$\begin{aligned} \Gamma^\theta{}_{r\theta} &= \Gamma^\theta{}_{\theta r} = \Gamma^\phi{}_{r\phi} = \Gamma^\phi{}_{\phi r} = \frac{1}{r}, & \Gamma^r{}_{\theta\theta} &= -r \\ \Gamma^\phi{}_{\theta\phi} &= \Gamma^\phi{}_{\phi\theta} = \cot\theta, & \Gamma^r{}_{\phi\phi} &= -r \sin^2\theta, & \Gamma^\theta{}_{\phi\phi} &= -\cos\theta \sin\theta. \end{aligned} \quad (2.10)$$

We take this affine connection eq. (2.10) as the suitable affine connection for static spherically symmetric spacetime in $f(Q)$ theory and hence the equation of motion (2.7) becomes [68, 69],

$$\begin{aligned}\kappa\mathcal{T}_{tt} &= \frac{e^{A-B}}{2r^2} \left\{ r^2 e^B f + 2f'_Q r (e^B - 1) + f_Q \left[(e^B - 1)(2 + rA') + (1 + e^B)rB' \right] \right\}, \\ \kappa\mathcal{T}_{rr} &= \frac{-1}{2r^2} \left\{ r^2 e^B f + 2f'_Q r (e^B - 1) + f_Q \left[(e^B - 1)(2 + rA' + rB') - 2rA' \right] \right\}, \\ \kappa\mathcal{T}_{\theta\theta} &= -\frac{r}{4e^B} \left\{ f_Q \left[-4A' - r(A')^2 - 2rA'' + rA'B' + 2e^B(A' + B') \right] + 2e^B r f - 2f'_Q r A' \right\},\end{aligned}\tag{2.11}$$

where $Q = \frac{(e^{-B}-1)(A'+B')}{r}$ and $f'_Q = f_{QQ} \frac{dQ}{dr}$. By solving eq. (2.11) with a concrete $f(Q)$ form and boundary conditions, we can obtain configurations $A(r)$ and $B(r)$. For example, if we consider vacuum solutions, this is $\mathcal{T}_{\mu\nu} = 0$, then eq. (2.11) gives us $A'(r) + B'(r) = 0$. Eq. (2.11) can be expressed as a set of equations containing the Tolman-Oppenheimer-Volkov equations for $f(Q)$ gravity, which describe the structure of neutron stars, along with the continuity equation given by the energy-momentum conservation of $\mathcal{T}_{\mu\nu}$ as,

$$\begin{aligned}A'' &= \frac{2e^B \left(r(f(Q) + 2p\kappa) + f_Q (A' + B') \right) - A' \left(f_Q (4 + rA' - rB') + 2f_{QQ} r Q' \right)}{2f_Q r}, \\ B' &= \frac{-\kappa e^B (p + \rho) r + f_Q A'}{f_Q}, \\ p' &= -\frac{(p + \rho)}{2} A'.\end{aligned}\tag{2.12}$$

It is important to note that the conservation of energy-momentum in $f(Q)$ gravity with the spherical symmetric metric form remains an issue [69, 71]. This issue is further discussed in Appendix A. By using the EoS and providing initial values for A , B , Q , ρ , and p , we can now describe the structure of neutron stars in $f(Q)$ gravity. If we set $f(Q) = Q$ in eq. (2.12), we can easily obtain the GR case solution (see Appendix B). From these equations, we can calculate the structure of neutron stars using various models.

3 $f(Q)$ Models

In the study of neutron star structure within the framework of $f(Q)$ gravity, we consider quadratic, exponential and logarithmic $f(Q)$ models. These models modify the gravitational action by introducing nonlinear functions of the nonmetricity scalar Q , thereby altering the equations governing the stellar structure. By analyzing these models, we aim to understand the impact of such modifications on the properties of neutron stars.

3.1 $f(Q) = Q + \alpha Q^2$

To explore the effects of different $f(Q)$ models, we first consider the specific model given by [17]:

$$f(Q) = Q + \alpha Q^2,\tag{3.1}$$

where α is the parameter for the quadratic nonmetricity correction. This specific choice is the simplest one and it is inspired in the Starobinsky model in $f(R)$ gravity, which has this same functional form. This quadratic term is particularly suitable for neutron star cases that exhibit strong gravity regimes. Conversely, the linear term typically applies to low gravity regimes. Additionally, this model is a special case of the more general power-law form of $f(Q)$, where:

$$f(Q) = Q + \alpha Q^n, \quad (3.2)$$

with $n = 2$. While the power-law form with different values of n could offer a broader range of behaviors and insights, numerical difficulties were encountered when working with values other than $n = 2$. Therefore, for the purposes of this paper, we focus on the Q^2 case. This choice allows for a more manageable numerical treatment while still capturing essential aspects of the modifications to gravity in the strong field regime relevant to neutron stars. With substitute eq. (3.1) to eq. (2.12), we can get the TOV equations as,

$$\begin{aligned} A'' &= \frac{2e^B r(Q + Q^2\alpha + 2p\kappa) + 2e^B(1 + 2\alpha)(A' + B')}{2(r + 2r\alpha)} \\ &\quad + \frac{A' \left(-((1 + 2\alpha)(4 + rA' - rB')) - 4r\alpha Q' \right)}{2(r + 2r\alpha)}, \\ B' &= \frac{e^B r\kappa(p + \rho)}{1 + 2Q\alpha} - A'. \end{aligned} \quad (3.3)$$

We can easily revert the eq. (3.2) to the GR case by setting the parameter $\alpha = 0$. Previous study [68] have discussed this model, demonstrating good consistency in both interior and exterior solutions using a polytropic equation. Moreover, the parameter α has an important role in generating the mass of neutron stars, where positive values of α yield smaller masses and negative values yield larger masses. In this paper, we re-examine the Q^2 model using more realistic EoS.

3.2 $f(Q) = Q + \alpha e^{\beta Q}$

Having derived the quadratic model, we now turn our calculation to another $f(Q)$ model, specifically the exponential form given by [23]:

$$f(Q) = Q + \alpha e^{\beta Q}, \quad (3.4)$$

where β and α are the parameters for the exponential correction term. According to [23], the exponential model provides slightly better fits to cosmological data than the concordance model. Also the exponential function allows us to explore more complex non-linear effects in strong gravitational fields, such as those found in neutron stars. Additionally, this model is connected to scalar-tensor theories and has been used in cosmology or large scale structure [27, 72]. Here we little modify the model for avoiding numerical problem from our TOV. The exponential model can capture details in areas with strong gravity that linear or quadratic models might miss. Moreover, the parameters α and β can be adjusted to better match observations. Specifically, β controls the rate of exponential growth, allowing

for precise adjustments, while α scales the overall amplitude of the exponential correction, providing broader modifications to the model. These parameters help in achieving a stable neutron star solution that fits with observational constraints. Because of its versatility feature, the exponential model $f(Q) = Q + \alpha e^{\beta Q}$ is a good choice for studying the structure of neutron stars. Using eq. (2.12), we can derive the TOV equations for this model as,

$$\begin{aligned}
A'' &= \frac{A' \left(-4 + 2e^B + rB' + e^{Q\beta} \alpha \beta \left(-4 + 2e^B + rB' - 2r\beta Q' \right) \right)}{2 \left(r + e^{Q\beta} r \alpha \beta \right)} \\
&\quad + \frac{2e^B \left(Qr + 2pr\kappa + B' + e^{Q\beta} \alpha \left(r + \beta B' \right) \right) - A'^2 r \left(1 + e^{Q\beta} \alpha \beta \right)}{2 \left(r + e^{Q\beta} r \alpha \beta \right)}, \\
B' &= \frac{e^B \kappa r (p + \rho)}{1 + e^{Q\beta} \alpha} - A'. \tag{3.5}
\end{aligned}$$

We can easily revert eq. (3.4) to the GR case by setting the parameters $\alpha = 0$. This ensures that the solutions obtained are consistent with the standard GR in the absence of modifications.

3.3 $f(Q) = Q - \alpha \ln(1 - \beta Q)$

In addition to the quadratic and exponential models, the logarithmic model is also considering. This model has been well-tested for explaining cosmological phenomena and dark energy [73]. Here we consider

$$f(Q) = Q - \alpha \ln(1 - \beta Q), \tag{3.6}$$

Geometrically, logarithmic model was successful in predicting the cosmic late-time accelerated expansion, and it is also a strong candidate for solving the cosmological constant problem. Moreover this model is effective in compressing the correction terms, which allows for the creation of more stable neutron stars with higher masses compared to the quadratic model. Similar to the exponential model, the parameters α and β have effects in adjusting the model to fit observational data accurately. Specifically, α affects the rate at which the logarithmic function approaches its critical point, and β scales the impact of the logarithmic term. This flexibility benefits the logarithmic model in achieving stable and good solutions for the structure of neutron stars. From eq. (2.12), we can derive the modified TOV as,

$$\begin{aligned}
A'' &= \frac{e^B \alpha (-1 + Q\beta) \ln(1 - Q\beta)}{1 - Q\beta + \alpha \beta} + \frac{(-1 + Q\beta)(Q + 2p\kappa)r + B'(-1 + Q\beta - \alpha\beta)}{(-1 + Q\beta - \alpha\beta)e^{-B}} - \frac{A'^2}{2} \\
&\quad + A' \left(\frac{-2 + e^B}{r} + \frac{B'}{2} - \frac{\alpha \beta^2 Q'}{(-1 + Q\beta)(-1 + Q\beta - \alpha\beta)} \right), \\
B' &= \frac{e^B \kappa r (-1 + Q\beta)(p + \rho)}{-1 + Q\beta - \alpha\beta} - A'. \tag{3.7}
\end{aligned}$$

By setting $\beta = 0$, we can recover GR case for this model. In the following sections, we will analyze how these three models influences the structure of neutron stars and evaluate its compatibility with observational data using realistic EoS.

4 Neutron Star Structure for $f(Q)$ Models

Using the TOV equations derived for each model, we perform numerical calculations to obtain the interior and exterior profiles of the neutron stars. Through these calculations, we can see how nonmetricity affects the structure of the stars. Furthermore, we calculate the mass-radius relation for each model, comparing these results with observational constraints to test the consistency of the $f(Q)$ models.

4.1 Boundary and Junction Conditions

To solve our ODE systems for all the $f(Q)$ models, we have three equations:

$A'' = f_1(Q, Q', B, B', p, \rho, r)$, $B' = f_2(Q, B, A', p, \rho, r)$, and $p' = f_3(A', p, \rho)$. Unlike the GR case, where the term Q' vanishes because $f_{QQ} = 0$, in all three models, we need an additional equation Q' that can be derived from eq. (2.11) to decouple the behavior of our ODE system. This allows us to set initial values for our ODE systems. In this discussion, we use the following initial values [68]:

$$B = 0, \quad A' = 0, \quad A = A_0, \quad Q = 0, \quad p = p_c. \quad (4.1)$$

The constant A_0 can be determined by matching the interior and exterior solutions of the star. As discussed in the covariant formulation of $f(Q)$, the condition $A' + B' = 0$ in vacuum implies that $Q(r) = 0$ outside the star. By evaluating eq. (2.11) under vacuum conditions, we can obtain:

$$e^B(2f_Q + f(Q)r^2) - 2f_Q(1 + rA') = 0.$$

Given the relationship $A'(r) + B'(r) = 0$ and $e^{A(r)} = e^{-B(r)}$, which can be easily derived from eq. (2.11), we can obtain the exterior solution of the star as:

$$e^{-B(r)} = e^{A(r)} = 1 + \frac{C}{r} + \frac{f(Q)|_0}{6f_Q|_0} r^2, \quad (4.2)$$

where C is an integration constant. This solution is similar to the Schwarzschild-de Sitter (SdS) solution with the cosmological constant $\Lambda = \frac{f(Q)|_0}{2f_Q|_0}$. When we apply the three $f(Q)$ models, the models given by Eqns. (3.1) and (3.6) will result in the same exterior solution as in GR, because the third term in eq. (4.2) will vanish. However, in the case of eq. (3.3), the third term does not vanish. A similar solution can also be obtained from eq.(2.7) by directly using the vacuum condition and $Q(r) = 0$. These solutions provide a boundary condition at the surface of the star that ensures the correct asymptotic behavior at infinity. The surface of the star can be determined by applying the boundary condition on the pressure. At the surface, the pressure of the star approaches zero, which can be defined as

$$p(r_s) \approx 0, \quad (4.3)$$

where r_s is the radius of the star at its surface. Another important aspect to consider is the junction condition for solving the equations between the interior and exterior solutions of these ODEs, addressing the transition. Since we are not considering any additional scalar

fields, and as seen in eq. (2.7), which still contains a term proportional to the Einstein tensor $G_{\mu\nu}$, we can apply the GR junction conditions. These conditions are given by $[h_{\mu\nu}] = 0$ and $[K_{\mu\nu}] = 0$ [74, 75]. The notation [...] specifically indicates the jump or discontinuity across the surface. The condition $[h_{\mu\nu}] = 0$ implies that the induced metric must be continuous across the hypersurface. On the other hand, $[K_{\mu\nu}] = 0$ indicates that there should be no discontinuity in the extrinsic curvature across the hypersurface. This condition ensures that the embedding of the hypersurface in the spacetime does not introduce any physical inconsistencies or abrupt changes. If we look at other modified gravity models such as $f(R)$ [76–78], we also need to pay attention to the continuity of nonmetricity. In this case, since we only have Q' in our TOV equations, it is necessary that $[Q] = 0$ so we can assume that there is no delta-function-like discontinuity. From eq. (4.2), the exterior solution is identical to the GR case, except for the exponential model which will be discussed later. This allows us to use the same junction conditions as in GR. This condition is also applied in the study of $f(Q)$ gravity on other compact objects. For instance, in [79, 80], the SdS solution is used as the exterior solution for strange star cases, and the same conditions apply to the interior and exterior boundaries. In other cases of charged isotropic compact stars, such as [81], the RdS (Reissner-Nordström-de Sitter) solution is used as the exterior solution, with a similar procedure applied for the junction condition between the interior and exterior solutions. In these cases, we only consider non-charged stars, so the RdS solution will have the same form as the SdS solution. For the mass of stars (m), we use explicitly the following equation refer to [68]:

$$m = 4\pi \int_0^{r_s} \rho(r)r^2 dr. \quad (4.4)$$

To solve the ODEs numerically, we also need to use dimensionless physical variables. We rescale using the gravitational radius r_g , so that the physical variables become,

$$\hat{r} \rightarrow \frac{r}{r_g}, \quad \hat{p} \rightarrow \frac{p}{p_g}, \quad \hat{\rho} \rightarrow \frac{\rho}{\rho_g}, \quad \hat{Q} \rightarrow Qr_g^2, \quad \hat{m} \rightarrow \frac{m}{M_\odot}, \quad (4.5)$$

where

$$r_g = \frac{GM_\odot}{c^2}, \quad p_g = \frac{M_\odot c^2}{r_g^3}, \quad \rho_g = \frac{M_\odot}{r_g^3}. \quad (4.6)$$

In this context, M_\odot represents the mass of the Sun, c denotes the speed of light, and G be the gravitational constant. All these constants are expressed in the cgs unit system, where $M_\odot \approx 1.989 \times 10^{33}$ g, $c \approx 2.997 \times 10^{10}$ cm/s, and $G \approx 6.674 \times 10^{-8}$ dyne.cm²/g². Another problem arises from the singularity behavior in our TOV equations. To avoid this, we expand eq. (2.12) around $r = 0$, obtaining the asymptotic solution near the center of the stars. This expansion helps in preventing singularities during the numerical integration. For the EoS, we used SLy [82, 83] tabulation¹. We also used the piece-wise polytrope form of APR4 [84] and MS1b [85], utilizing tabulation parameters from [86]. A fixed three-piece fit is implemented at $10^{14.7}$ g/cm³ and 10^{15} g/cm³ for both EoS. By using these EoS, we can achieve a more realistic modeling of the pressure-density relations ($p = p(\rho)$) within

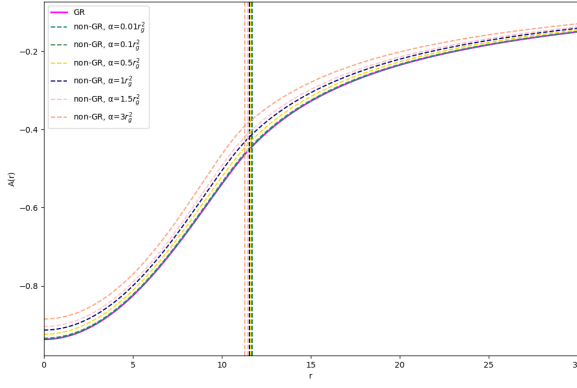
¹Tabulated SLy EoS can be obtained from <http://www.ioffe.ru/astro/NSG/NSEOS/>.

neutron stars. After doing the numerical setting, we can now solve the ODE systems. We use the RK45 method, which can dynamically adjust the step size to balance accuracy and computational efficiency, with the `scipy.integrate.solve_ivp` package in Python to numerically integrate the ODEs and obtain the solutions. This package allows for flexible and efficient solving of initial value problems for ODEs.

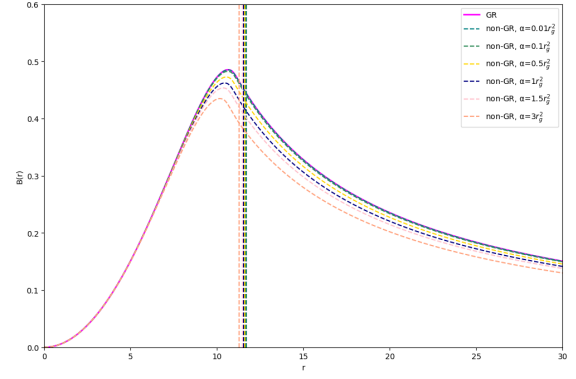
4.2 Numerical Solutions

We compute the structure of neutron stars and the mass-radius diagrams for the nonmetricity formulation. Due to numerical limitations in our TOV equations, we will only calculate for positive α for the Q^2 model. The solutions of the TOV equations for all three models are illustrated in figure 1 and figure 2. As shown in these figures, the central pressure of the star rapidly drops to zero. This boundary condition allows us to determine the surface of the star (r_s) where $p(r_s) \approx 0$. Due to numerical reasons, we set $p(r_s) \leq 10^{-8}p_c$ for determining r_s . At this radius, we identify the boundary of the star and solve the junction conditions between the interior and exterior solutions of the star. In this study, we only consider SdS solution for the exterior of the stars. Using eq. (4.2) at the vacuum condition, we determine C using the shooting method simultaneously with A_0 . For $f(Q) = Q + \alpha Q^2$ and $f(Q) = Q - \alpha \ln(1 - \beta Q)$, we can easily get $\Lambda = 0$, but for $f(Q) = Q + \alpha e^{\beta Q}$, $\Lambda \neq 0$, which will make the exterior solution of the exponential model different. This is because $f(Q)|_0 = \alpha$, so it is obtained that $\Lambda = \frac{\alpha}{2(1+\alpha\beta)}$. However, since $\alpha = \hat{\alpha}/r_g^2$ for the exponential model, the constant r_g^2 compresses the third term of the SdS solution, resulting in an exterior solution similar to the other two models as illustrated in figure 1. This process ensures continuity for the metric functions $B(r)$ and $A(r)$ between interior and exterior solution. In the figures, we can see also that the exterior solutions $B(r)$ and $A(r)$ naturally converge to zero as $r \rightarrow \infty$ because $1 + \frac{C}{r}$ exterior solution.

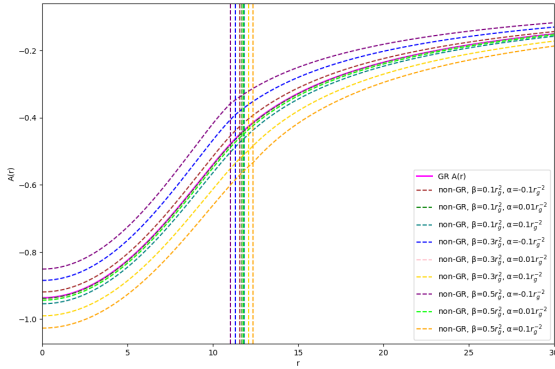
Next, we turn our attention to the behavior of the nonmetricity profile $Q(r)$, which is illustrated in figure 2b, 2d, 2f. For $f(Q) = Q + \alpha Q^2$, the nonmetricity decreases as α increases. This is the opposite of the other two models, where a positive α results in a more dominant nonmetricity compared to the GR case. Specifically, in the Q^2 model, Q^2 is positive while Q is negative. This solution aligns with the solutions for $B(r)$ and $A(r)$. By calculating $Q_{rrr} = e^B B'$, we observe that the value of $B(r)$ can decrease as $Q(r)$ decreases, suggesting that a larger α results in a smaller $B(r)$. On the other hand, the behavior of $A(r)$ is consistent with the solutions for Q_{rtt} , where $A(r)$ becomes smaller as $Q(r)$ decreases. This indicates that the nonmetricity has important role in the formation of the structure of neutron stars. This conclusion is strengthened by the neutron star mass-radius diagram which will be discussed further in the next subsection. This behavior is also consistent with previous study related to solutions for $A(r)$, $B(r)$, and $Q(r)$. However, there is a slight difference where previous studies found that $Q(r)$ values were larger for positive α in the Q^2 model. We expect this different result arises because we used all field equations to obtain the TOV equations. Our results of all three models show the consistent relationship between $Q(r)$, $A(r)$, and $B(r)$.



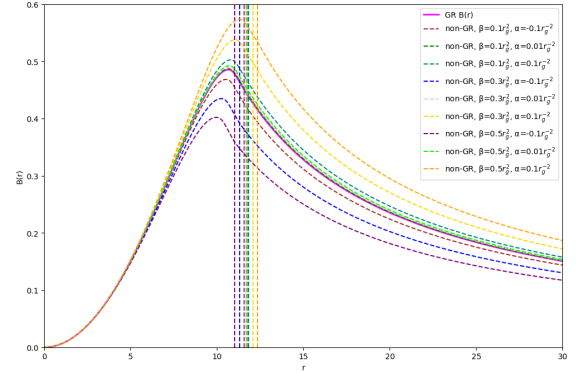
(a) Metric Component of $A(r)$ for $f(Q) = Q + \alpha Q^2$



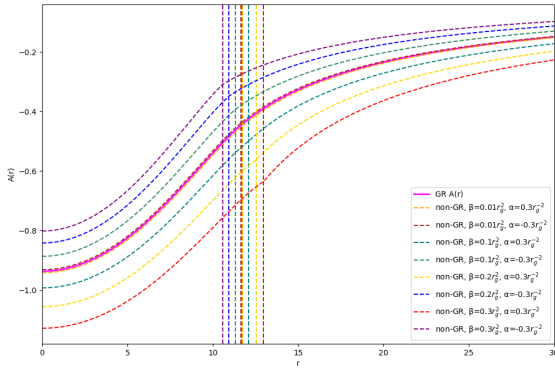
(b) Metric Component of $B(r)$ for $f(Q) = Q + \alpha Q^2$



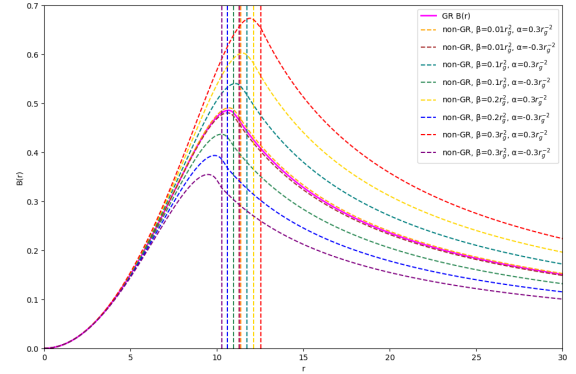
(c) Metric Component of $A(r)$ for $f(Q) = Q + \alpha e^{\beta Q}$



(d) Metric Component of $B(r)$ for $f(Q) = Q + \alpha e^{\beta Q}$

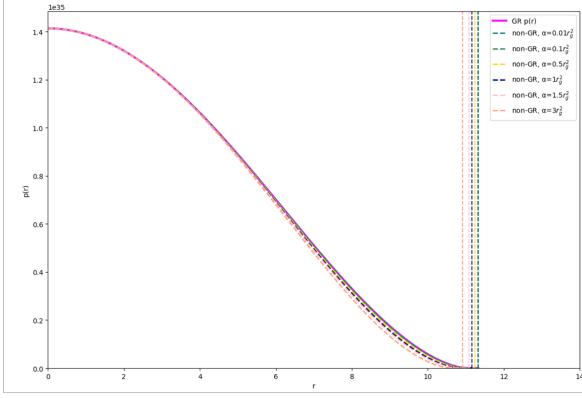


(e) Metric Component of $A(r)$ for $f(Q) = Q - \alpha \ln(1 - \beta Q)$

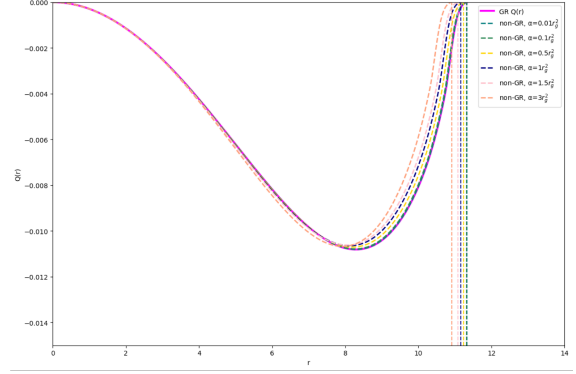


(f) Metric Component of $B(r)$ for $f(Q) = Q - \alpha \ln(1 - \beta Q)$

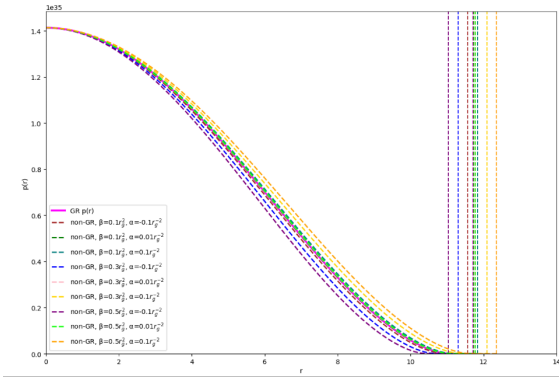
Figure 1: Metric solutions for the $f(Q)$ models with various parameters α and β using $\rho_c = 1 \times 10^{15}, \text{g/cm}^3$ (SLy EoS). r is in km unit. The parameters α and β affect the deviation in each solution. The vertical dashed lines indicate the r_{surface} for each set of parameters. We can see that for small values of $\alpha = 0.01r_g^2$ and $\alpha = 0.01r_g^{-2}$, the Q^2 and exponential models closely match the GR case. Similarly, for the logarithmic model, setting a very small parameter $\beta = 0.01r_g^{-2}$ also allows it to match the GR case. The functions $A(r)$ and $B(r)$ are connected from the interior metric to the exterior metric using the SdS solution at the r_s .



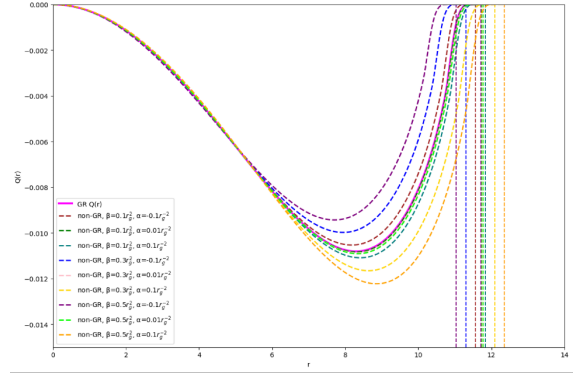
(a) Pressure profile of $A(r)$ for $f(Q) = Q + \alpha Q^2$



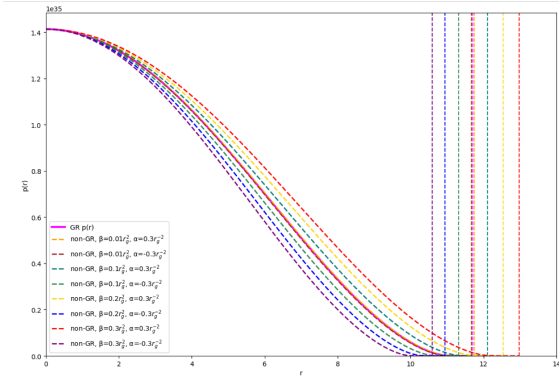
(b) nonmetricity Profile of $Q(r)$ for $f(Q) = Q + \alpha Q^2$



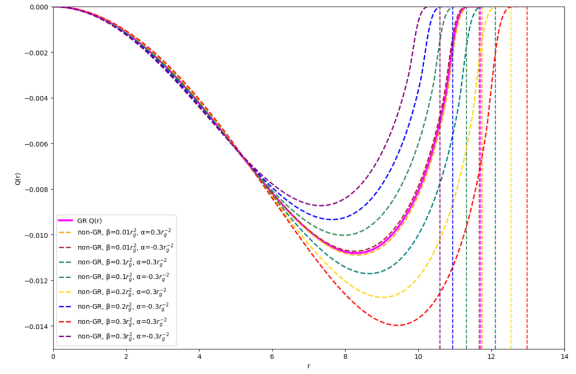
(c) Pressure profile of $p(r)$ for $f(Q) = Q + \alpha e^{\beta Q}$



(d) nonmetricity Profile of $Q(r)$ for $f(Q) = Q + \alpha e^{\beta Q}$



(e) Pressure profile of $p(r)$ for $f(Q) = Q - \alpha \ln(1 - \beta Q)$



(f) nonmetricity Profile of $Q(r)$ for $f(Q) = Q - \alpha \ln(1 - \beta Q)$

Figure 2: Nonmetricity and pressure profile for the $f(Q)$ models with various parameters α and β using $\rho_c = 1 \times 10^{15}, g/cm^3$ (SLy EoS). $p(r)$ is in $dyne/cm^2$ unit, $Q(r)$ is in r_g^{-2} unit, and r is in km unit. The vertical dashed lines indicate the r_{surface} for each set of parameters. The profiles of $Q(r)$ and $p(r)$ approaching zero at the surface boundary match the exterior solutions of $A(r)$ and $B(r)$.

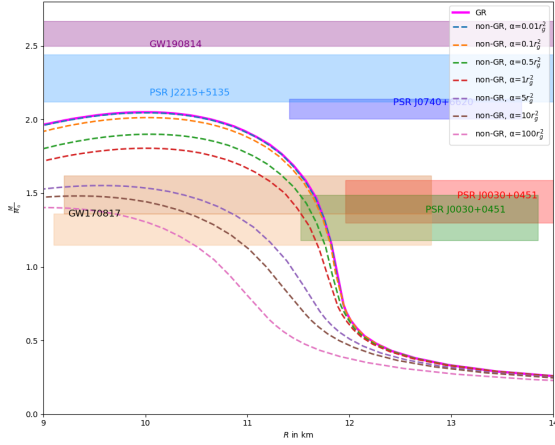
4.3 Mass-Radius Relation

By repeating the structure calculation of a neutron star over a range of central density values (ρ_c), we obtained mass-radius diagrams for several parameter values across all models. The plot also includes various observational constraints from GW events and massive pulsars. GW events detected by LIGO-Virgo, starting with the first event GW170817 [45] and subsequent events like GW190814 [46], are believed to involve neutron stars with masses around $2.59 \pm 0.08 M_\odot$. Besides GW events, we also use observational constraints from massive pulsars such as PSR J2215+5135 [87], one of the most massive neutron stars, obtained through radio and optical observations with a mass of $2.27^{+0.17}_{-0.15} M_\odot$. Another observational constraint we utilize comes from NICER, such as PSR J0030+0451, with two sets of observational results indicating mass estimates. Miller et al. estimated the mass to be $1.34^{+0.15}_{-0.16} M_\odot$ with a radius of $12.71^{+1.14}_{-1.19}$ km [42], while Riley et al. estimated the mass to be $1.44^{+0.15}_{-0.14} M_\odot$ with a radius of $13.02^{+1.24}_{-1.06}$ km [88]. The differences between these estimates arise from different assumptions and modeling approaches regarding the thermal emission from the hot spots on the surface of neutron stars. Another massive pulsar from NICER that reported a radius measurement based on fits of rotating hot spot patterns to NICER and X-ray Multi-Mirror (XMM-Newton) X-ray observations is PSR J0740+6620. Miller et al. reported a mass of $2.08 \pm 0.07 M_\odot$ and a radius of $13.7^{+2.6}_{-1.5}$ km [43], while Riley et al. reported a mass of $2.072^{+0.067}_{-0.066} M_\odot$ and a radius of $12.39^{+1.30}_{-0.98}$ km [44], using informative priors on pulsar mass, distance, and orbital inclination derived from joint NANOGrav and CHIME/Pulsar wide-band radio timing measurements. In this study, we use the observational constraint from [44]. The results of the mass-radius ($\mathcal{M} - \mathcal{R}$) diagram for the Q^2 model show a decrease in mass as the positive α value increases, as illustrated in figure 3. These results are consistent with previous study [68]. Furthermore, examining the mass-central density ($\mathcal{M} - \rho_c$) diagram in figure 3d, the behavior aligns with results from the study using a polytropic EoS, where the mass of star tends to be similar at low ρ_c values. We get also similar result for the other two models. These plots show similarities in the $\mathcal{M} - \mathcal{R}$ and $\mathcal{M} - \rho_c$ diagrams for $f(Q)$ and $f(T)$ gravity theories [89, 90]. Unfortunately, using the TOV equations (eq. 3.3), the solutions obtained are not stable enough to form a star with negative α . Therefore, to satisfy the observational constraints in the Q^2 model with positive α , we need a stiffer EoS like MS1b. When using SLy and APR4 EoS (figure 3a, figure 3b), it is observed that only the GW170817 constraint is met. However, when applying a very stiff EoS like MS1b (figure 3c), the mass-radius diagram meets the constraints of GW190814, PSR J2215+5135, PSR J0740+6620, and PSR J0030+0451 across various values of α .

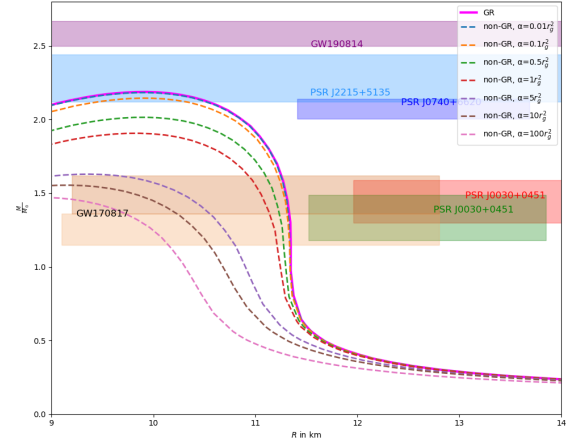
Because we cannot generate larger stars than GR for negative α in the Q^2 model, we try to use another model to compress the correction terms in $f(Q)$, such as $f(Q) = Q + \alpha e^{\beta Q}$ and $f(Q) = Q + \alpha \ln(1 - \beta Q)$, where the exponential and logarithmic terms are expected to compress the correction terms and yield stable neutron stars. In figure 4, the $\mathcal{M} - \mathcal{R}$ diagram follows the same pattern as the GR case and shows more stable stars compared to the Q^2 plot for higher masses. When α increases positively, a more massive star is obtained. On the other hand, if α decreases negatively, the star becomes less massive. The same behavior is also can be obtained with the β parameter if we use same value of α : when β is positive, a

more massive star is obtained, whereas when β is negative, we get less massive than in the GR case.

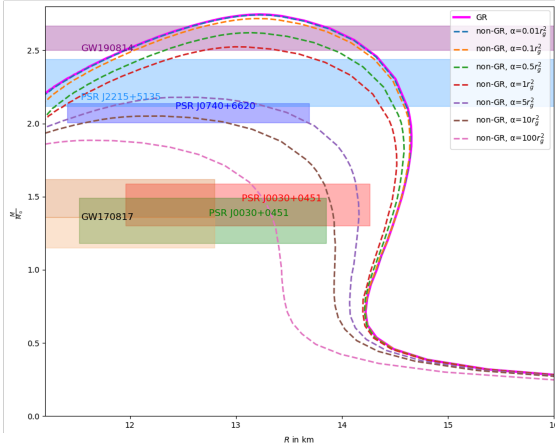
As we said in the previous section, α acts as coarse tuning and β as fine tuning. α controls the magnitude of the exponential correction in $f(Q)$, directly affecting the amplitude of the corrections introduced by the exponential term. Therefore, changing the value of α results in significant changes in the structure of the star. The β parameter controls the growth rate of the exponential function, influencing the details of the nonlinear corrections in the gravitational field. By adjusting α and β together, we can fine-tune the desired structure of the star.



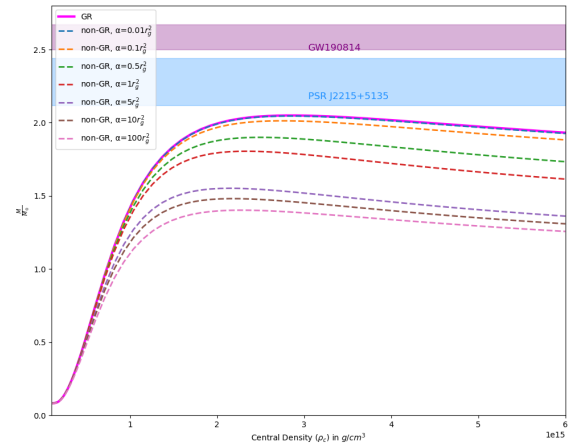
(a) Mass-Radius Diagram for SLy EoS



(b) Mass-Radius Diagram for APR4 EoS

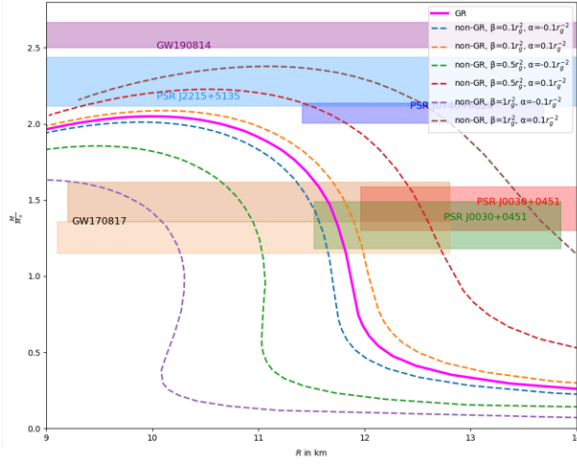


(c) Mass-Radius Diagram for MS1b EoS

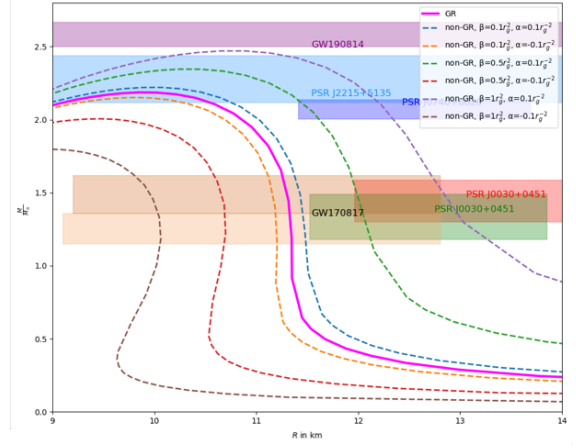


(d) Mass- ρ_c Diagram for SLy EoS

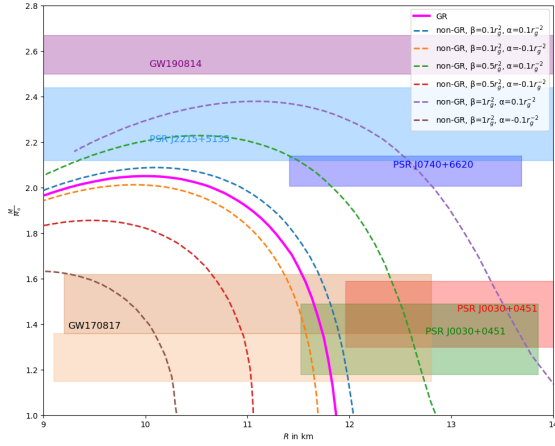
Figure 3: Mass-radius and mass- ρ_c diagrams for $f(Q) = Q + \alpha Q^2$ using realistic EoS, SLy, APR4, and MS1b. The values of α range from $0.01r_g^2$ to $100r_g^2$. The plot also includes various observational constraints: GW190814, PSR J2215+5135, PSR J0740+6620, GW170817, and PSR J0030+0451. It can be observed that for small values of α , specifically $0.01r_g^2$, the diagram matches the GR case.



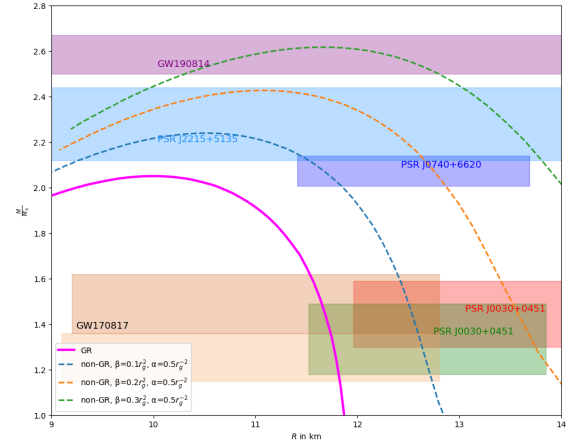
(a) Mass-Radius Diagram for SLy EoS



(b) Mass-Radius Diagram for APR4 EoS

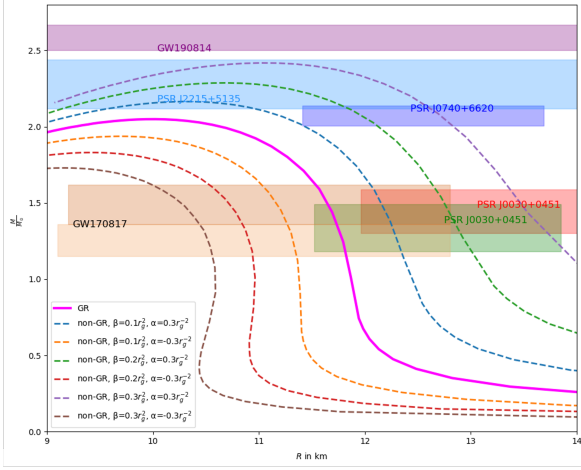


(c) The zoomed-in plot mass-radius diagram for $\alpha = [0.1, -0.1]r_g^{-2}$ and $\beta = [0.1, 0.5, 0.1]r_g^{-2}$ using SLy EoS

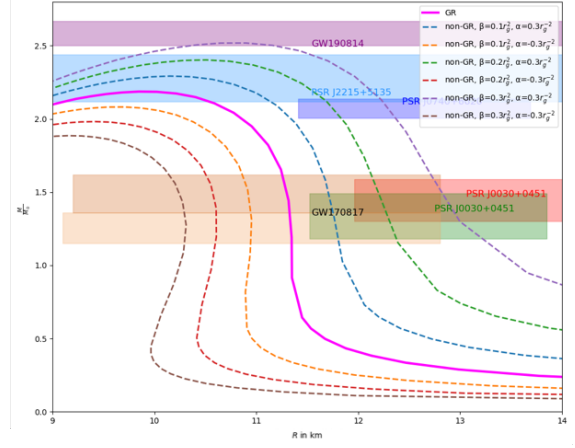


(d) The zoomed-in plot mass-radius diagram for $\alpha = 0.5r_g^{-2}$ and $\beta = [0.1, 0.2, 0.3]r_g^{-2}$ using SLy EoS

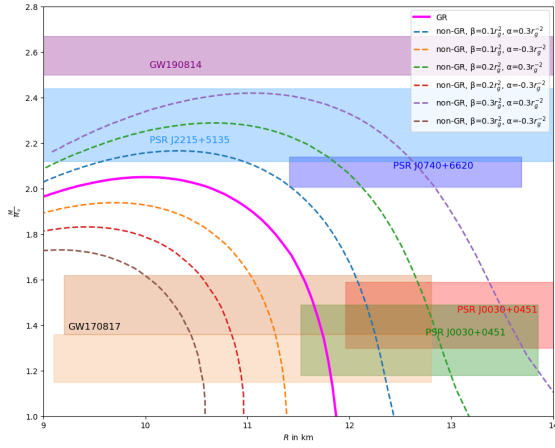
Figure 4: Mass-Radius diagrams for $f(Q) = Q + \alpha e^{\beta Q}$ using realistic EoS, SLy and APR4. The plot also includes various observational constraints: GW190814, PSR J2215+5135, PSR J0740+6620, GW170817, and PSR J0030+0451. The zoomed-in plots shows the roles of tuning parameters α and β . In β tuning, it is observed that changes in β from 0.1, 0.5, and 1 result in slight variations in the mass of the neutron star, which are not significant. We can compare with α tuning, for $\alpha = 0.5r_g^{-2}$, it is possible to achieve a star mass that satisfies the GW190814 constraint. When tuning, it is important to adjust the α and β combination so that the star remains stable.



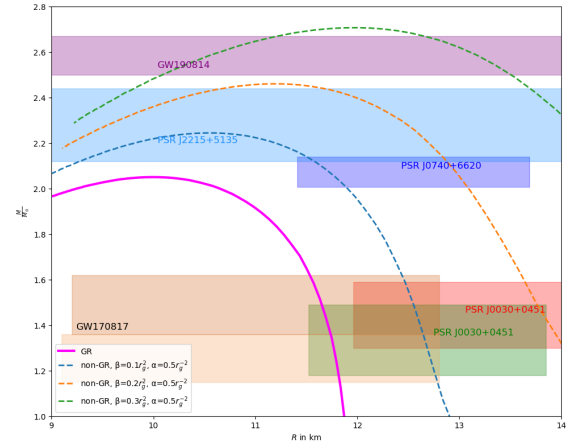
(a) Mass-Radius Diagram for SLy EoS



(b) Mass-Radius Diagram for APR4 EoS



(c) The zoomed-in plot Mass-Radius diagram for $\alpha = [0.3, -0.3]r_g^{-2}$ and $\beta = [0.1, 0.2, 0.3]r_g^{-2}$ using SLy EoS



(d) The zoomed-in plot Mass-Radius diagram for $\alpha = 0.5r_g^{-2}$ and $\beta = [0.1, 0.2, 0.3]r_g^{-2}$ using SLy EoS

Figure 5: Mass-Radius diagrams for $f(Q) = Q - \alpha \ln(1 - \beta Q)$ using realistic EoS, SLy and APR4. The plot also includes various observational constraints: GW190814, PSR J2215+5135, PSR J0740+6620, GW170817, and PSR J0030+0451. The zoomed-in plots shows the roles of tuning parameters α and β . In β tuning, it is observed that changes in β from 0.1 to 1 result in slight variations in the mass of the neutron star, which are not significant. We can compare with α tuning, for $\alpha = 0.5r_g^{-2}$, it is possible to achieve a star mass that satisfies the GW190814 constraint.

Table 1: Using the different α and β values in the $f(Q)$ model, the maximum mass (\mathcal{M}_{Max}), the radius (\mathcal{R}), their ratios represent the compactness (\mathcal{C}), and the redshift parameter (z_s) of the Neutron stars for the SLy EoS.

$f(Q)$ Model	α	β	\mathcal{M}_{Max}	\mathcal{R}	\mathcal{C}	z_s
$Q + \alpha Q^2$	GR		2.05	9.995	0.205	0.302
	0.01		2.046	9.989	0.205	0.302
	0.1		2.013	10.044	0.200	0.291
	0.5		1.900	10.032	0.189	0.268
	1		1.805	10.029	0.180	0.250
	5		1.552	9.545	0.163	0.218
	10		1.481	9.346	0.158	0.209
	100		1.402	8.987	0.156	0.206
$Q + \alpha e^{\beta Q}$		0.1	2.012	9.8895	0.203	0.297
	-0.1	0.5	1.855	9.460	0.196	0.282
		1	1.632	8.947	0.182	0.254
	GR		2.05	9.995	0.205	0.302
		0.1	2.087	10.098	0.207	0.306
	0.1	0.5	2.227	10.531	0.211	0.315
		1	2.378	11.053	0.215	0.325
		0.1	2.238	10.515	0.213	0.320
	0.5	0.2	2.426	11.048	0.220	0.336
		0.3	2.616	11.663	0.224	0.346
		0.1	2.429	11.078	0.219	0.334
		0.2	2.826	12.294	0.230	0.361
$Q - \alpha \ln(1 - \beta Q)$		0.1	1.937	9.702	0.200	0.291
	-0.3	0.2	1.831	9.406	0.195	0.280
		0.3	1.73	9.164	0.189	0.268
	GR		2.05	9.995	0.205	0.302
		0.1	2.165	10.310	0.210	0.313
	0.3	0.2	2.288	10.690	0.214	0.322
		0.3	2.418	11.027	0.219	0.334
		0.1	2.244	10.529	0.213	0.320
	0.5	0.2	2.459	11.172	0.220	0.336
		0.3	2.706	12.009	0.225	0.348
		0.1	2.447	11.206	0.218	0.332
		0.2	2.968	12.964	0.229	0.358

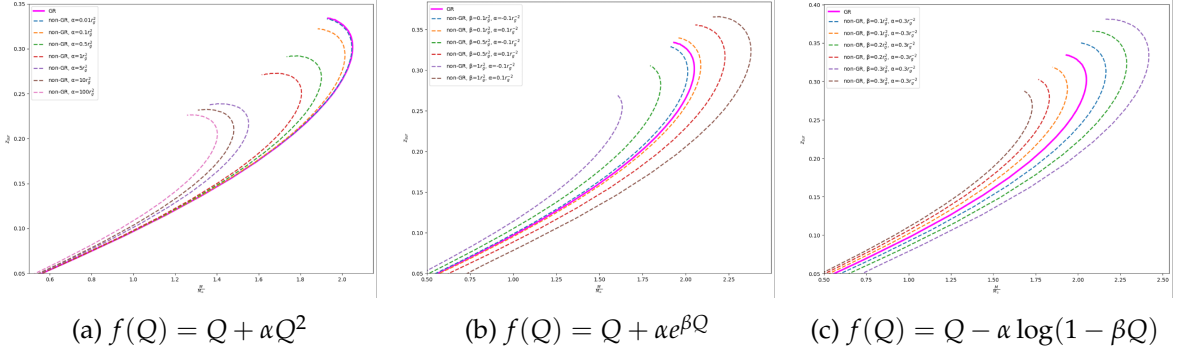


Figure 6: The surface gravitational redshift z_s function of M/M_\odot for each $f(Q)$ model. In this plot, we use SLy EoS and some parameter α and β . From this plot, we can see z_s fulfill constraint from [91].

As shown in figures 4c, when adjusting the β parameter with $\alpha = 0.1r_g^{-2}$, there is a smooth change in the mass of star. In contrast, in figure 4d with $\alpha = 0.5r_g^{-2}$ at the same β value, the change in the mass of star is more significant and can reach the observational constraint for the possibly most massive star GW190814. The significant role of α is also visible when returning the $f(Q)$ equation to GR at very small alpha values such as $\alpha = 0.01r_g^{-2}$ as in figure 1c, 1d, 2c and 2d.

In the model $f(Q) = Q - \alpha \ln(1 - \beta Q)$, we obtained results that has similar behavior to the exponential model. As shown in figure 5, with positive α , we obtain more massive stars, and with negative α , we obtain less massive stars than in the GR case. At certain parameter values, it can be seen that the diagram meets GW190814, PSR J2215+5135, PSR J0740+6620, GW170817, and PSR J0030+0451 constraints.

Both α and β play important roles in this model as we explained in the previous section. α controls the effect of the logarithmic term, while β determines the critical point and the rate of decrease of the logarithmic function. It is evident that when β is very small, the solution converges to the GR solution. The effect of these two parameters can also be seen in figure 5c and figure 5d. When adjusting $\alpha = 0.5r_g^{-2}$ with $\beta = 0.3r_g^2$, we can achieve sufficiently massive stars that meet the GW190814 constraint. In both models, using $\alpha = 2r_g^{-2}$, we can get massive stars $>2.75M_\odot$ at small β values such as $\beta = 0.1r_g^2$. However, we encounter numerical difficulties at low central densities for this parameter value. Careful tuning of these two parameters is required for both models because the star can become very unstable if the exponential or logarithmic terms are too large.

The other neutron star properties that we can obtain from mass-radius relation are compactness (\mathcal{C}) and surface gravitational redshift (z_s). Now, \mathcal{C} can be defined as,

$$\mathcal{C} = \mathcal{M}/\mathcal{R}. \quad (4.7)$$

Buchdal [91] has provided the upper limit for the compactness of neutron star, which will remain stable if the value $\leq \frac{4}{9}$. For z_s , defined as $\frac{1}{\sqrt{-g_{tt}}} - 1$, the Λ term in g_{tt} at the surface of the star in the SdS solution can be ignored, as discussed in subsection 4.2. The Λ term

becomes zero for the quadratic and logarithmic models, and can be neglected for the exponential model due to the r_g constant suppresses the Λ term. Therefore, we can use the same definition of z_s from GR as,

$$z_s = \frac{1 - \sqrt{1 - 2\mathcal{C}}}{\sqrt{1 - 2\mathcal{C}}}. \quad (4.8)$$

According to Refs. [91] and [92], the surface gravitational redshift must satisfy $z_s \leq 2$ for neutron stars. Both \mathcal{C} and z_s have been shown in Table 1 and figure 6. As shown in Table 1, the two parameters, α and β , have different roles in star compactness in the exponential and logarithmic models. In both models, α and β affect compactness, with α acting as coarse tuning having a larger effect than β , which acts as fine tuning. Compactness increases with the increasing values of both parameters, and vice versa. The z_s for both the models are also consistent with the $\mathcal{M} - \mathcal{R}$ diagram, where positive α results in a larger z_s and negative α results in a smaller z_s . From figure 6, we can see that at low mass, z_s values do not differ significantly, but at higher mass, the deviation in z_s due to parameter differences becomes more pronounced. For the quadratic model, we can also observe how compactness and z_s decrease with increasing α . From the table, we can conclude that all configurations satisfy the neutron star compactness and z_s limits.

5 Discussion

After obtaining the solutions for the structure of each star and the mass-radius relationship of neutron stars in covariant $f(Q)$ gravity, we can observe that nonmetricity has an important role in star formation. Looking at the results from $f(Q) = Q + \alpha Q^2$, we find that the star becomes lighter as α increases. This reduction in mass is accompanied by a decrease in the profile of $Q(r)$, indicating a correlation between Q and the ability of star to acquire matter. Unfortunately, using the TOV equations [eq. (3.3)], the solutions obtained are not stable enough to form a star with negative α . Furthermore, we have also tried using higher-order corrections, such as $f(Q) = Q + \alpha Q^2 + \beta Q^n$, but the results remain the same. These models still cannot generate higher masses, indicating that they are unable to compress the Q^2 corrections sufficiently to achieve higher mass configurations. This limitation may be due to the inability of the higher-order terms to effectively counteract the dominant Q^2 term, leading to insufficient structural changes to support a more massive star. Previous works on $f(Q)$ and $f(T)$ gravity [68, 90] have shown that for negative α , a critical point for stability cannot be found. For positive α , the modified gravity terms tend to stabilize the star by allowing configurations with less massive stars compared to the GR case. When α is negative, the nonmetricity function $f(Q)$ introduces significant deviations from GR, affecting the equilibrium of the star. These changes can indirectly affect the structure of star, allowing it to hold more mass. However, this alteration in structure can make the star unstable, especially when the central density and energy density exceed a certain threshold. This instability prevents the formation of stable neutron stars with negative α , as the changes to the structure of star disrupt the balance needed to keep it stable. We found different results with the other two models. In these models, the additional terms in $f(Q)$ can effectively

compress the value of $|Q|$, allowing the both more massive and less massive stars without issues. However, the parameters α and β are important for maintaining the stability of the structure of star.

Moreover, if we look at the $\mathcal{M} - \rho_c$ diagram in figure 3d, the modification effect of gravity is not significant at low central density, so the results are similar to GR. As the central density increases, modified $f(Q)$ begin to affect the structure of star, causing changes in mass and radius. This corresponds to [93], which indicates that at low energies, the effects of modified gravity will not be very visible because the solution obtained will return to GR.

So, from the solutions of all models, we can opine that the nonmetricity in the star affects the geometry of the interior structure of the star, which consists of perfect fluid. Thus affecting the distribution of pressure and matter. When the profile $Q(r)$ starts to deviate due to changes in the parameters α and β , the profile $B(r)$ also starts to deviate. The metric tensor coefficient $e^{B(r)}$ is related to the mass function of the star through the equation $e^{-B(r)} = 1 - \frac{2m(r)}{r}$. Therefore, any deviations in $B(r)$ will directly affect the interior mass function $m(r)$. When $B(r)$ deviates due to $Q(r)$, the star can either accommodate more matter or less matter, impacting the total mass. This change in matter distribution is also accompanied by pressure deviations due to changes in $A(r)$. Strong gravity in the core pulls the matter of star inward, attempting to compress it, while internal pressure generated by nuclear reactions and degeneracy pressure counteracts this gravitational pull to prevent collapse. The deviation $A(r)$ due to $Q(r)$ changes this balance by changing the internal pressure. If the pressure increases, the star can support more mass and remain stable. Conversely, if the pressure decreases, the star loses matter, leading to a decrease in total mass. Thus, the stability of the star is closely tied to the deviations in both $A(r)$ and $B(r)$ caused by $Q(r)$.

We can find a similar phenomenon in how $f(Q)$ affects the pressure distribution in strange stars [94], where the radial and tangential pressures inside the star are influenced by nonmetricity. In these stars, anisotropic fluids are used, and as $|Q|$ increases, the nonmetricity scalar changes the interior structure of the star, leading to an increase in both radial and tangential pressures. A similar effect can be found in other references, such as the $f(T)$ model [95] or previous studies on $f(Q)$ [68] that used a polytropic EoS for their calculations. These studies explain how torsion in $f(T)$ or nonmetricity in $f(Q)$ affects the geometric fluid, impacting the pressure and enabling the star to accommodate more matter. Therefore, this scenario is also possible in the context of our study.

6 Conclusions

In this paper, we have studied neutron stars in covariant $f(Q)$ gravity using three modified $f(Q)$ models: $f(Q) = Q + \alpha Q^2$; $f(Q) = Q + \alpha e^{\beta Q}$; and $f(Q) = Q - \alpha \ln(1 - \beta Q)$. By using piecewise polytrope EoS, we obtained the metric profiles $A(r)$ and $B(r)$, nonmetricity $Q(r)$, and pressure $p(r)$ in the interior of the star, which match the exterior SdS solution outside the star. We also calculated $\mathcal{M} - \mathcal{R}$ diagram of neutron stars. The parameters α and β have their respective roles in each model in influencing the structure of the star.

In the model $f(Q) = Q + \alpha Q^2$, the profile $Q(r)$ decreases as the positive value of α increases. This affects the profiles of $A(r)$ and $B(r)$, influencing the mass and compactness of the star. Our results show that as α increases, the star becomes less massive and less compact. Previous studies also have shown that with negative α , it is possible to obtain more massive neutron stars. However, with the TOV equations we used, we could not generate stable neutron stars with negative α , which we suspect is due to the instability in the Q' term when controlling the αQ^2 correction. In the models $f(Q) = Q + \alpha e^{\beta Q}$ and $f(Q) = Q - \alpha \ln(1 - \beta Q)$, we successfully obtained neutron stars that are more massive and compact compared to those in GR. The parameter α controls the influence of the correction term, while the parameter β acts as a fine-tuning parameter for the exponential or logarithmic growth rate. By carefully tuning these parameters to small values, we can modify the structure of star to achieve more massive or less massive stars. Using SLy and APR4 EoS, the resulting $\mathcal{M} - \mathcal{R}$ diagrams meet the constraints from GW190814, PSR J2215+5135, PSR J0740+6620, GW170817, and PSR J0030+0451. For example, in the logarithmic model, with $\beta = 0.3r_g^2$ and $\alpha = 0.3r_g^{-2}$, the $\mathcal{M} - \mathcal{R}$ diagram meets all observational constraints when using the APR4 EoS. In contrast to the $f(Q) = Q + \alpha Q^2$ model with positive α which requires a very stiff EoS such as MS1b to satisfy observational constraints. Careful tuning of α and β parameters is necessary to avoid stellar instability because achieving higher masses just requires small parameter values. Additionally, as shown in Table 1, all configurations satisfy the neutron star compactness and z_s limit, $\mathcal{C} \leq \frac{4}{9}$ and $z_s \leq 2$.

From all results, it can be observed that Q has important role in the structure of neutron star matter. In summary, the nonmetricity affects the internal geometry of the star, which in turn affects the density, pressure, and overall stability of the neutron star. This enables the star to accommodate more matter and withstand a heavier mass. It will also be interesting to consider hair solution for solving neutron stars in $f(Q)$ gravity. This approach may provide more comprehensive results and improve our understanding of the modifications introduced by gravity $f(Q)$ in the context of neutron star structure. This scenario has also been studied in various works related to $f(R)$ gravity in neutron stars [96–98]. Hair solution in $f(R)$ gravity has been shown to introduce additional stability and modify the exterior and interior solutions of stars, leading to a more comprehensive understanding of stellar structures under modified gravity theories. Moreover, considering more general solutions, as demonstrated in studies on black holes in $f(Q)$ gravity [99], by constructing the most general static and spherically symmetric forms of the metric and the affine connection, could provide further insights into the structure and stability of neutron stars.

Acknowledgments

The authors thank N. Yoshioka for the useful discussion. MAA would also like to thank M. D. Danarianto for his helpful discussion regarding numerical methods on neutron stars. BM thanks IUCAA, Pune (India) for providing support in the form of an academic visit during which this work is accomplished. SAN acknowledges the financial support provided by

Hiroshima University, Japan through Japan Student Services Organization (JASSO) Fellowship to carry out the research work.

A Energy-Momentum Conservation

One of the issues in $f(Q)$ gravity within the spherically symmetry metric is the conservation of energy-momentum. In accordance with Refs. [69] and [71], a constraint arises on the left-hand side when the covariant derivative is applied to eq. (2.7). Let's redefine eq. (2.7) where the left side represents the gravitational part as $E_{\mu\nu}$, and the right side represents the matter part, $\mathcal{T}_{\mu\nu}$.

$$E_{\mu\nu} \equiv f_Q \overset{\circ}{G}_{\mu\nu} + \frac{1}{2} g_{\mu\nu} (Q f_Q - f) + 2 f_{QQ} P^\lambda{}_{\mu\nu} \overset{\circ}{\nabla}_\lambda Q = \kappa \mathcal{T}_{\mu\nu}. \quad (\text{A.1})$$

As discussed in [69], the right side, under the assumption of energy-momentum conservation, can easily become zero when the covariant derivative is applied, $\overset{\circ}{\nabla}_\mu \mathcal{T}^{\mu\nu} = 0$. However, the covariant derivative of the left side, representing the gravitational part, will give a constraint as:

$$\frac{(e^B - 1)(4 + rA' + rB') + 2rB'}{2r^2} f'_Q + \frac{(e^B - 1)}{r} f''_Q = 0, \quad (\text{A.2})$$

where $f'_Q = f_{QQ} \frac{dQ}{dr} = f_{QQ} Q'$ and $f''_Q = f_{QQQ} \left(\frac{dQ}{dr}\right)^2 + f_{QQ} \frac{d^2 Q}{dr^2} = f_{QQQ} Q'^2 + f_{QQ} Q''$. So eq. (A.2) becomes

$$\begin{aligned} & \left[\frac{(e^B - 1)(4 + rA' + rB') + 2rB'}{2r^2} \right] f_{QQ} Q' + \frac{(e^B - 1)}{r} (f_{QQQ} Q'^2 + f_{QQ} Q'') = 0 \\ & f_{QQ} \left[\frac{(e^B - 1) rA' - (e^B + 1) rB' + 4(e^B - 1)}{2r^2} Q' + \frac{e^B - 1}{r} Q'' \right] \\ & \quad + f_{QQQ} \left[\frac{e^B - 1}{r} Q'^2 \right] = 0 \\ & f_{QQ} \Phi_r + f_{QQQ} \Psi_r = 0 \quad (\text{A.3}) \end{aligned}$$

We can see that $\overset{\circ}{\nabla}_\mu E^{\mu\nu}$ gives constraint that are zero only when Q is constant or $B = 0$. Unfortunately, this scenario is not possible in the case of neutron stars, as shown in figures 1 and 2, which illustrate the profiles of $B(r)$ and $Q(r)$. Therefore, we calculated the constraint on $\overset{\circ}{\nabla}^\mu E_{\mu\nu}$ numerically. The results are shown in figure 7. Here, we describe $f_{QQ} \Phi_r$, $f_{QQQ} \Psi_r$, and $\overset{\circ}{\nabla}_\mu E^{\mu\nu}$ for each model. The numerical plot illustrates that at the center and the surface of star, the constraint are zero due to the absence of nonmetricity. However, between the core and the surface, the constraint are non-zero but very small, ranging from the smallest order of 10^{-17} in the quadratic model to the largest order of 10^{-9} in the logarithmic model. From these results, it is still reasonable to assume $\overset{\circ}{\nabla}_\mu \mathcal{T}^{\mu\nu} \approx 0$, considering the constraint yields only very small values. Furthermore, in the neutron star calculations, particularly in

the continuity equation, we focus on the matter part described by the EoS, which allows us to neglect these very small constraint term, thus enabling the use of the continuity equation in eq. (2.12) for neutron star calculations.

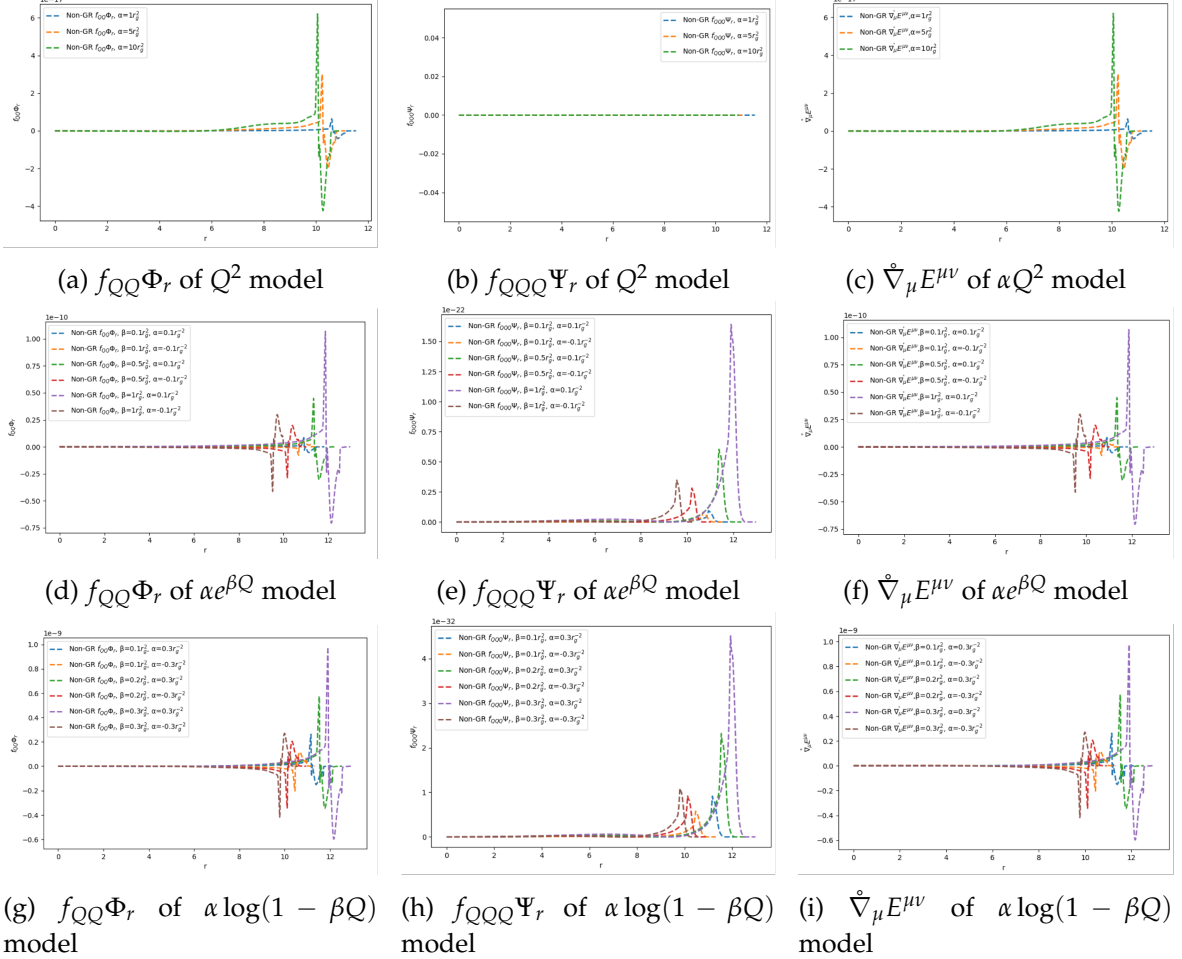


Figure 7: $f_{QQ}\Phi_r$, $f_{QQQ}\Psi_r$, and $\overset{\circ}{\nabla}_\mu E^{\mu\nu}$ for each model using SLy EoS. In this plot, we use $\rho_c = 1 \times 10^{15}$ g/cm³. Note that the quadratic model has no f_{QQQ} term. These plots demonstrate that $\overset{\circ}{\nabla}_\mu E^{\mu\nu}$ for each model is very small, with the largest value in the logarithmic model reaching the order of 10^{-9} . Additionally, these results are consistent with analytical calculations, showing that at the core and surface of the star, $\overset{\circ}{\nabla}_\mu E^{\mu\nu} = 0$ due to the absence of nonmetricity.

B Recovering TOV GR

The instability behaviour arises from our solutions, so we want to make sure that the TOV equations are capable of recovering to GR after setting $\alpha = 0$. We will attempt to recover GR by two methods. In the first case, we will directly recover from eq. (2.11), and in the second case, we will calculate the solution when $\alpha = 0$ in eq. (3.3). After setting $f(Q) = Q$ the eq.

(2.11) become

$$\begin{aligned}\kappa e^A \rho &= \frac{e^{A-B}}{2r^2} \left\{ r^2 e^B Q + \left[(e^B - 1)(2 + rA') + (1 + e^B)rB' \right] \right\}, \\ \kappa e^B p &= \frac{-1}{2r^2} \left\{ r^2 e^B Q + \left[(e^B - 1)(2 + rA' + rB') - 2rA' \right] \right\}.\end{aligned}\tag{B.1}$$

By substitute the covariant Q , we will get

$$8\pi\rho r^2 = 1 - e^{-B}(1 - rB'),\tag{B.2}$$

$$8\pi p r^2 = -1 + e^{-B}(1 + rA').\tag{B.3}$$

Integrating (B.2), we obtain:

$$e^{-B} = 1 - \frac{2m}{r}.\tag{B.4}$$

Substituting this relation into (B.2) and (B.3), and using the mass distribution in spherical coordinates, we get

$$A' = \frac{\frac{m}{r^2} + 4\pi p(r)r}{1 - \frac{2m}{r}}.\tag{B.5}$$

Using the continuity equation from eq. (2.12), we can derive the TOV equation in GR as:

$$\frac{dp}{dr} = \frac{(p + \rho)}{2m - r} \left(\frac{m}{r} + 4\pi p(r)r^2 \right).\tag{B.6}$$

References

- [1] A.G. Riess, A.V. Filippenko, P. Challis, A. Clocchiatti et al., *Observational Evidence from Supernovae for an Accelerating Universe and a Cosmological Constant*, *Astron. J.* **116** (1998) 1009.
- [2] S. Perlmutter, G. Aldering, G. Goldhaber, R.A. Knop et al., *Measurements of Ω and Λ from 42 High-Redshift Supernovae*, *Astrophys. J.* **517** (1999) 565.
- [3] P.A.R. Ade, N. Aghanim, M. Arnaud, M. Ashdown et al., *Planck 2015 results: XIII. Cosmological parameters*, *Astron. Astrophys.* **594** (2016) 63.
- [4] N. Aghanim, M. Arnaud, M. Ashdown, J. Aumont et al., *Planck 2015 results: XI. CMB power spectra, likelihoods, and robustness of parameters*, *Astron. Astrophys.* **99** (2016) 594.
- [5] J.B. Jiménez, L. Heisenberg and T.S. Koivisto, *The Geometrical Trinity of Gravity*, *Universe* **5** (2019) 173.
- [6] J. Harada, *Connection independent formulation of general relativity*, *Phys. Rev. D* **101** (2020) 024053.
- [7] R. Aldrovandi and J.G. Pereira, *Teleparallel Gravity: An Introduction*, vol. 173, Springer (2013), 10.1007/978-94-007-5143-9.
- [8] J.W. Maluf, *The teleparallel equivalent of general relativity*, *Annalen Phys.* **525** (2013) 339.
- [9] J.M. Nester and H.-J. Yo, *Symmetric teleparallel general relativity*, *Chinese J. Phys.* **37** (1999) 113.
- [10] M. Adak, M. Kalay and O. Sert, *Lagrange formulation of the symmetric teleparallel gravity*, *Int. J. Mod. Phys. D* **15** (2006) 619.

- [11] M. Adak, O. Sert, M. Kalay and M. Sari, *Symmetric Teleparallel Gravity: Some exact solutions and spinor couplings*, *Int. J. Mod. Phys. A* **28** (2013) 1350167.
- [12] I. Mol, *The Non-Metricity Formulation of General Relativity*, *Adv. Appl. Clifford Algebras* **27** (2017) 2607.
- [13] L. Järv, M. Rünkla, M. Saal and O. Vilson, *Nonmetricity formulation of general relativity and its scalar-tensor extension*, *Phys. Rev. D* **97** (2018) 124025.
- [14] J.B. Jiménez, L. Heisenberg and T. Koivisto, *Coincident general relativity*, *Phys. Rev. D* **98** (2018) 044048.
- [15] J.B. Jiménez, L. Heisenberg and T.S. Koivisto, *Teleparallel Palatini theories*, *JCAP* **08** (2018) 039.
- [16] V. Gakis, M. Krššák, J.L. Said and E.N. Saridakis, *Conformal gravity and transformations in the symmetric teleparallel framework*, *Phys. Rev. D* **101** (2020) 064024.
- [17] T. Harko, T.S. Koivisto, F.S.N. Lobo, G.J. Olmo and D. Rubiera-Garcia, *Coupling matter in modified Q gravity*, *Phys. Rev. D* **98** (2018) 084043.
- [18] R. Lazkoz, F.S.N. Lobo, M. Ortiz-Baños and V. Salzano, *Observational constraints of $f(Q)$ gravity*, *Phys. Rev. D* **100** (2019) 104027.
- [19] J. Lu, X. Zhao and G. Chee, *Cosmology in symmetric teleparallel gravity and its dynamical system*, *Eur. Phys. J. C* **79** (2019) 530.
- [20] J.B. Jiménez, L. Heisenberg, T. Koivisto and S. Pekar, *Cosmology in $f(Q)$ geometry*, *Phys. Rev. D* **101** (2020) 103507.
- [21] B.J. Barros, T. Barreiro, T. Koivisto and N.J. Nunes, *Testing $F(Q)$ gravity with redshift space distortions*, *Phys. Dark Universe* **30** (2020) 100616.
- [22] N. Frusciante, *Signatures of $f(Q)$ gravity in cosmology*, *Phys. Rev. D* **103** (2021) 044021.
- [23] F.K. Anagnostopoulos, S. Basilakos and E.N. Saridakis, *First evidence that non-metricity $f(Q)$ gravity could challenge Λ CDM*, *Phys. Lett. B* **822** (2021) 136634.
- [24] W. Khylllep, A. Paliathanasis and J. Dutta, *Cosmological solutions and growth index of matter perturbations in $f(Q)$ gravity*, *Phys. Rev. D* **103** (2021) 103521.
- [25] S.A. Narawade, L. Pati, B. Mishra and S. Tripathy, *Dynamical system analysis for accelerating models in non-metricity $f(Q)$ gravity*, *Phys. Dark Universe* **36** (2022) 101020.
- [26] S.A. Narawade and B. Mishra, *Phantom Cosmological Model with Observational Constraints in $f(Q)$ Gravity*, *Ann. Phys.* **535** (2023) 2200626.
- [27] S.A. Narawade, S.P. Singh and B. Mishra, *Accelerating cosmological models in $f(Q)$ gravity and the phase space analysis*, *Phys. Dark Universe* **42** (2023) 101282.
- [28] L. Heisenberg, *Review on $f(Q)$ gravity*, *Phys. Rept.* **1066** (2024) 1.
- [29] L. Heisenberg, M. Hohmann and S. Kuhn, *Cosmological teleparallel perturbations*, *JCAP* **03** (2024) 063.
- [30] S. Nojiri and S.D. Odintsov, *Well-defined $f(Q)$ gravity, reconstruction of FLRW spacetime and unification of inflation with dark energy epoch*, *Phys. Dark Universe* **45** (2024) 101538.
- [31] G. Subramaniam, A. De, T.-H. Loo and Y.K. Goh, *How different connections in flat FLRW geometry impact energy conditions in $f(Q)$ theory?*, *Fortschritte der Phys.* **71** (2023) 2300038.

- [32] H. Shabani, A. De and T.-H. Loo, *Phase-space analysis of a novel cosmological model in $f(Q)$ theory*, *Eur. Phys. J. C* **83** (2023) 535.
- [33] A. Paliathanasis, *Dynamical analysis of $f(Q)$ -cosmology*, *Phys. Dark Universe* **41** (2023) 101255.
- [34] N. Dimakis, A. Paliathanasis, M. Roumeliotis and T. Christodoulakis, *FLRW solutions in $f(Q)$ theory: The effect of using different connections*, *Phys. Rev. D* **106** (2022) 043509.
- [35] L. Heisenberg, M. Hohmann and S. Kuhn, *Homogeneous and isotropic cosmology in general teleparallel gravity*, *Eur. Phys. J. C* **83** (2023) 315.
- [36] H. Shabani, A. De, T.-H. Loo and E.N. Saridakis, *Cosmology of $f(Q)$ gravity in non-flat Universe*, *Eur. Phys. J. C* **84** (2024) 285.
- [37] G. Subramaniam, A. De, T.-H. Loo and Y.K. Goh, *Energy condition bounds on $f(Q)$ model parameters in a curved FLRW Universe*, *Phys. Dark Universe* **41** (2023) 101243.
- [38] P. Bhar and J.M.Z. Pretel, *Dark energy stars and quark stars within the context of $f(Q)$ gravity*, *Phys. Dark Universe* **42** (2023) 101322.
- [39] P. Bhar, K.N. Singh, S.K. Maurya and M. Govender, *A four parameters quark star in quadratic $f(Q)$ - action*, *Phys. Dark Universe* **43** (2024) 101391.
- [40] S. Kaur, S.K. Maurya, S. Shukla and B. Dayanandan, *Charged anisotropic fluid sphere in $f(Q)$ gravity satisfying Vaidya-Tikekar metric*, *New Astron.* **110** (2024) 102230.
- [41] M.Z. Gul, S. Rani, M. Adeel and A. Jawad, *Viable and stable compact stars in $f(Q)$ theory*, *Eur. Phys. J. C* **84** (2024) 8.
- [42] M.C. Miller, F.K. Lamb, A.J. Dittmann, S. Bogdanov et al., *PSR J0030+0451 Mass and Radius from NICER Data and Implications for the Properties of Neutron Star Matter*, *Astrophys. J. Lett.* **887** (2019) L24.
- [43] M.C. Miller, F.K. Lamb, A.J. Dittmann, S. Bogdanov et al., *The Radius of PSR J0740+6620 from NICER and XMM-Newton Data*, *Astrophys. J. Lett.* **918** (2021) L28.
- [44] T.E. Riley, A.L. Watts, P.S. Ray et al., *A NICER View of the Massive Pulsar PSR J0740+6620 Informed by Radio Timing and XMM-Newton Spectroscopy*, *Astrophys. J. Lett.* **918** (2021) L27.
- [45] B.P. Abbott, R. Abbott, T.D. Abbott, F. Acernese et al., *GW170817: Observation of Gravitational Waves from a Binary Neutron Star Inspiral*, *Phys. Rev. Lett.* **119** (2017) 161101.
- [46] R. Abbott, T.D. Abbott, S. Abraham, F. Acernese et al., *GW190814: Gravitational Waves from the Coalescence of a 23 Solar Mass Black Hole with a 2.6 Solar Mass Compact Object*, *Astrophys. J. Lett.* **896** (2020) L44.
- [47] J.M. Lattimer and M. Prakash, *The equation of state of hot, dense matter and neutron stars*, *Phys. Rep.* **621** (2016) 127.
- [48] K. Hebeler, J.M. Lattimer, C.J. Pethick and A. Schwenk, *Equation of State and Neutron Star Properties Constrained by Nuclear Physics and Observation*, *Astrophys. J.* **773** (2013) 11.
- [49] F. Özel and P. Freire, *Masses, Radii, and the Equation of State of Neutron Stars*, *Annu. Rev. Astron. Astrophys.* **54** (2016) 401.
- [50] A.W. Steiner, C.O. Heinke, S. Bogdanov, C.K. Li, W.C.G. Ho, A. Bahramian et al., *Constraining the mass and radius of neutron stars in globular clusters*, *Mon. Notices Royal Astron. Soc.* **476** (2018) 421.

- [51] B. Bertotti, A. Cavaliere and F. Pacini, *Rotating Neutron Stars and Pulsar Emission*, *nature* **221** (1969) 624.
- [52] A.W. Steiner, J.M. Lattimer and E.F. Brown, *THE NEUTRON STAR MASS-RADIUS RELATION AND THE EQUATION OF STATE OF DENSE MATTER*, *Astrophys. J.* **765** (2013) L5.
- [53] A.W. Steiner, S. Gandolfi, F.J. Fattoyev and W.G. Newton, *Using neutron star observations to determine crust thicknesses, moments of inertia, and tidal deformabilities*, *Phys. Rev. C* **91** (2015) 015804.
- [54] S. Chandrasekhar, *The Maximum Mass of Ideal White Dwarfs*, *Astrophys. J.* **74** (1931) 81.
- [55] M.L. Rawls, J.A. Orosz, J.E. McClintock, M.A.P. Torres, C.D. Bailyn and M.M. Buxton, *REFINED NEUTRON STAR MASS DETERMINATIONS FOR SIX ECLIPSING X-RAY PULSAR BINARIES**, *Astrophys. J.* **730** (2011) 25.
- [56] F. Mullally, C. Badenes, S.E. Thompson and R. Lupton, *TWINS: THE TWO SHORTEST PERIOD NON-INTERACTING DOUBLE DEGENERATE WHITE DWARF STARS*, *Astrophys. J.* **707** (2009) L51.
- [57] P.B. Demorest, T. Pennucci, S.M. Ransom, M.S.E. Roberts and J.W.T. Hessels, *A two-solar-mass neutron star measured using Shapiro delay*, *nature* **467** (2010) 1081.
- [58] N.-B. Zhang and B.-A. Li, *Implications of the Mass $M = 2.17^{+0.11}_{-0.10} M_{\odot}$ of PSR J0740+6620 on the Equation of State of Super-dense Neutron-rich Nuclear Matter*, *Astrophys. J.* **879** (2019) 99.
- [59] A. Ganguly, R. Gannouji, R. Goswami and S. Ray, *Neutron stars in the Starobinsky model*, *Phys. Rev. D* **89** (2014) 064019.
- [60] A.V. Astashenok, S. Capozziello and S.D. Odintsov, *Extreme neutron stars from Extended Theories of Gravity*, *JCAP* **01** (2015) 001.
- [61] S.S. Yazadjiev, D.D. Doneva, K.D. Kokkotas and K.V. Staykov, *Non-perturbative and self-consistent models of neutron stars in R-squared gravity*, *JCAP* **06** (2014) 003.
- [62] S. Capozziello, M. De Laurentis, R. Farinelli and S.D. Odintsov, *Mass-radius relation for neutron stars in $f(R)$ gravity*, *Phys. Rev. D* **93** (2016) 023501.
- [63] A.V. Astashenok, S.D. Odintsov and A. de la Cruz-Dombriz, *The realistic models of relativistic stars in $f(R) = R + \alpha R^2$ gravity*, *Class. Quant. Grav.* **34** (2017) 205008.
- [64] A.V. Kpadonou, M.J.S. Houndjo and M.E. Rodrigues, *Tolman-Oppenheimer-Volkoff equations and their implications for the structures of relativistic stars in $f(T)$ gravity*, *Astrophys. and Space Sci.* **361** (2016) 244.
- [65] M. Pace and J.L. Said, *A perturbative approach to neutron stars in $f(T, T)$ -gravity*, *Eur. Phys. J. C* **77** (2017) 283.
- [66] H.G.M. Fortes and J.C.N. Araujo, *Solving Tolman-Oppenheimer-Volkoff equations in $f(T)$ gravity: a novel approach*, *Class. Quant. Grav.* **39** (2022) 245017.
- [67] J.C.N. de Araujo and H.G.M. Fortes, *Solving Tolman-Oppenheimer-Volkoff equations in $f(T)$ gravity: A novel approach applied to some realistic equations of state*, *Int. J. Mod. Phys. D* **31** (2022) 2250101.
- [68] R.-H. Lin and X.-H. Zhai, *Spherically symmetric configuration in $f(Q)$ gravity*, *Phys. Rev. D* **103** (2021) 124001.
- [69] D. Zhao, *Covariant formulation of $f(Q)$ theory*, *Eur. Phys. J. C* **82** (2022) 303.

- [70] J.-T. Beh, T.-H. Loo and A. De, *Geodesic deviation equation in $f(Q)$ -gravity*, *Chinese J. Phys.* **77** (2022) 1551.
- [71] A. De and T.-H. Loo, *On the viability of $f(Q)$ gravity models*, *Classical and Quantum Gravity* **40** (2023) 115007.
- [72] O. Sokoliuk, S. Arora, S. Praharaj, A. Baransky and P.K. Sahoo, *On the impact of $f(Q)$ gravity on the large scale structure*, *Mon. Notices Royal Astron. Soc.* **522** (2023) 252.
- [73] J.A. Nájera, C.A. Alvarado and C. Escamilla-Rivera, *Constraints on $f(Q)$ logarithmic model using gravitational wave standard sirens*, *Mon. Notices Royal Astron. Soc.* **524** (2023) 5280.
- [74] W. Israel, *Singular hypersurfaces and thin shells in general relativity*, *Nuovo cimento B* **44S10** (1966) 1.
- [75] D. Marolf and S. Yaida, *Energy conditions and junction conditions*, *Phys. Rev. D* **72** (2005) 044016.
- [76] N. Deruelle, M. Sasaki and Y. Sendouda, *Junction Conditions in $f(R)$ Theories of Gravity*, *Prog. theor. phys.* **119** (2008) 237.
- [77] J.M.M. Senovilla, *Junction conditions for $F(R)$ -gravity and their consequences*, *Phys. Rev. D* **88** (2013) 064015.
- [78] W.-X. Feng, C.-Q. Geng, W.F. Kao and L.-W. Luo, *Equation-of-state of neutron stars with junction conditions in the Starobinsky model*, *Int. J. of Modd. Phys. D* **27** (2017) 1750186.
- [79] S.K. Maurya, K.N. Singh, S.V. Lohakare and B. Mishra, *Anisotropic Strange Star Model Beyond Standard Maximum Mass Limit by Gravitational Decoupling in $f(Q)$ Gravity*, *Fortschritte der Phys.* **70** (2022) 2200061.
- [80] S.K. Maurya, K.N. Singh et al., *The Effect of Gravitational Decoupling on Constraining the Mass and Radius for the Secondary Component of GW190814 and Other Self-bound Strange Stars in $f(Q)$ Gravity Theory*, *Astrophys. J., Suppl. Ser.* **269** (2023) 35.
- [81] S. Chaudharya, S.K. Maurya, J. Kumara and G. Mustafa, *Most general isotropic charged fluid solution for Buchdahl model in $\mathcal{F}(Q)$ gravity*, [arXiv:2406.18604](https://arxiv.org/abs/2406.18604).
- [82] F. Douchin and P. Haensel, *A unified equation of state of dense matter and neutron star structure*, *Astron. Astrophys.* **380** (2001) 151.
- [83] A.Y. Potekhin, A.F. Fantina, N. Chamel, J.M. Pearson and S. Goriely, *Analytical representations of unified equations of state for neutron-star matter*, *Astron. Astrophys.* **560** (2013) A48.
- [84] A. Akmal, V.R. Pandharipande and D.G. Ravenhall, *Equation of state of nucleon matter and neutron star structure*, *Phys. Rev. C* **58** (1998) 1804.
- [85] H. Müller and B.D. Serot, *Relativistic mean-field theory and the high-density nuclear equation of state*, *Nucl. Phys. A* **606** (1996) 508.
- [86] J.S. Read, B.D. Lackey, B.J. Owen and J.L. Friedman, *Constraints on a phenomenologically parametrized neutron-star equation of state*, *Phys. Rev. D* **79** (2009) 124032.
- [87] M. Linares, T. Shahbaz and J. Casares, *Peering into the Dark Side: Magnesium Lines Establish a Massive Neutron Star in PSR J2215+5135*, *Astrophys. J.* **859** (2018) 54.
- [88] T.E. Riley, A.L. Watts, S. Bogdanov et al., *A NICER View of PSR J0030+0451: Millisecond Pulsar Parameter Estimation*, *Astrophys. J. Lett.* **887** (2019) L21.
- [89] M.G. Ganiou, C. Aïnamon, M.J.S. Houndjo and J. Tossa, *Strong magnetic field effects on neutron stars within $f(T)$ theory of gravity*, *Eur. Phys. J. Plus* **132** (2017) 250.

- [90] S.c.v. Ilijić and M. Sossich, *Compact stars in extended theory of gravity*, *Phys. Rev. D* **98** (2018) .
- [91] H.A. Buchdahl, *General relativistic fluid spheres*, *Phys. Rev.* **116** (1959) 1027.
- [92] V. Müller, N. Straumann: *General relativity and relativistic astrophysics*. Springer-Verlag, Berlin, Heidelberg, New York, Tokyo 1984. XIII + 459 Seiten. DM 112,-, *Astronomische Nachrichten* **308** (1987) 40.
- [93] W. Barker and S. Zell, *Consistent particle physics in metric-affine gravity from extended projective symmetry*, [arXiv:2402.14917](https://arxiv.org/abs/2402.14917).
- [94] S.V. Lohakare, S.K. Maurya, K.N. Singh, B. Mishra and A. Errehymy, *Influence of three parameters on maximum mass and stability of strange star under linear $f(Q)$ – action*, *Mon. Notices Royal Astron. Soc.* **526** (2023) 3796.
- [95] R.-H. Lin, X.-N. Chen and X.-H. Zhai, *Realistic neutron star models in $f(T)$ gravity*, *Eur. Phys. J. C* **82** (2022) 308.
- [96] A.V. Astashenok, A.S. Baigashov and S.A. Lapin, *Neutron stars in frames of R^2 –gravity and gravitational waves*, *Int. J. Geom. Methods Mod. Phys.* **16** (2019) 1950004.
- [97] P. Feola, X.J. Forteza, S. Capozziello, R. Cianci and S. Vignolo, *Mass-radius relation for neutron stars in $f(R) = R + \alpha R^2$ gravity: A comparison between purely metric and torsion formulations*, *Phys. Rev. D* **101** (2020) 044037.
- [98] K. Numajiri, Y.-X. Cui, T. Katuragawa and S. Nojiri, *Revisiting compact star in $F(R)$ gravity: Roles of chameleon potential and energy conditions*, *Phys. Rev. D* **107** (2023) 104019.
- [99] F. D’Ambrosio, S.D.B. Fell, L. Heisenberg and S. Kuhn, *Black holes in $f(Q)$ gravity*, *Phys. Rev. D* **105** (2022) 024042.